

Review

Review and perspective of materials for flexible solar cells

Xiaoyue Li^{a,b}, Peicheng Li^b, Zhongbin Wu^b, Deying Luo^{b,c}, Hong-Yu Yu^c, Zheng-Hong Lu^{a,b,c,*}^a Department of Physics, Center for Optoelectronics Engineering Research, Yunnan University, Kunming, 650091, PR China^b Department of Materials Science and Engineering, University of Toronto, Toronto, Ontario, M5G 3E4, Canada^c School of Microelectronics, Southern University of Science and Technology, Shenzhen, 518055, PR China

ARTICLE INFO

Keywords:

Flexible solar cells
Substrates
Electrodes
Organic semiconductors
Polymers
Perovskites
Silicon

ABSTRACT

Thin-film flexible solar cells are lightweight and mechanically robust. Along with rapidly advancing battery technology, flexible solar panels are expected to create niche products that require lightweight, mechanical flexibility, and moldability into complex shapes, such as roof-panel for electric automobiles, foldable umbrellas, camping tents, etc. In this paper, we provide a comprehensive assessment of relevant materials suitable for making flexible solar cells. Substrate materials reviewed include metals, ceramics, glasses, and plastics. For active materials, we focus primarily on emerging new semiconductors including small organic donor/acceptor molecules, conjugated donor/acceptor polymers, and organometal halide perovskites. For electrode materials, transparent conducting oxides, thin metal films/nanowires, nanocarbons, and conducting polymers are reviewed. We also discuss the merits, weaknesses, and future perspectives of these materials for developing next-generation flexible photovoltaics.

1. Introduction

Combustion of fossil fuel dominates today's power generation and, alarmingly, 38% of total world electricity supply still relies on burning coal in 2019. Renewable energy sources such as solar, wind, rain, tides, and geothermal heat have enormous potential to replace conventional fossil fuels in the future. Sunlight has long been identified as the most promising sustainable source of clean energy and thus solar cells have been actively researched over the past decades. Global cumulatively installed photovoltaics (PVs) capacity is expected to reach 512 GW, providing energy for the rapidly growing population around the world. After decades of R&D and aided by government subsidies, the average price per watt for PV panel has dropped from ~\$100 in 1975 to ~\$3 today. For most solar factory operations, installation of polysilicon-based panels has become a profitable business. For example, a solar PV establishment in the city of Seville, Spain, generates enough electricity for 6000 households annually; and the world's largest solar farm built in Temgger Desert, China, houses a huge array of solar panels covering 248

acres generating electricity around 1500 MW annually.

In the late 1970s, amorphous silicon thin-film solar cells were first used for powering hand-held calculators. Thin-film solar-cell modules are lightweight and flexible as compared with modules built by traditional crystalline silicon cells. Moreover, thin-film cells may be easily molded into various shapes and sizes based on the need of a specific application. The mechanically tough and yet flexible modules made from thin-film cells offer an extremely attractive energy source solution for many outdoor products of which the total weight and mechanically impact resilience is crucial. For example, numerous automobile companies have started integrating solar panels on the roofs of electric cars as a supplementary source of charging. As shown in Fig. 1, a Toyota Prius has solar panels integrated on engine compartment hood, passenger cabin roof, and cargo cabin door. Umbrella made with flexible solar panels potentially provides energy sources for night illumination and for charging various mobile gadgets such as phones and laptop PCs (right panel of Fig. 1). With rapid progress in recent years in new material systems, such as organic semiconductors and metal halide perovskites, flexible PV panels are expected to be commercialized in many more future marketable products. Already the revenue share of thin-film cells has exceeded 25% of the total PV market. Together with new generations of lightweight energy storage devices, such as batteries and supercapacitors, thin-film solar cells are expected to be integrated into many future mobile and flexible devices providing a sustainable energy source for charging electronic equipment ranging from electric cars, electric bicycles, to smartphones and portable computers.

The various materials used to build a flexible thin-film cell are shown

* Corresponding author. Department of Materials Science and Engineering, University of Toronto, Toronto, Ontario, M5G 3E4, Canada.

E-mail address: zhenghong.lu@utoronto.ca (Z.-H. Lu).



Production and Hosting by Elsevier on behalf of KeAi

<https://doi.org/10.1016/j.matre.2020.09.001>

Received 26 March 2020; Accepted 29 June 2020

Available online 1 October 2020

2666-9358/© 2020 Chongqing Xixin Tianyuan Data & Information Co., Ltd. Publishing services by Elsevier B.V. on behalf of KeAi Communications Co. Ltd. This is an

open access article under the CC BY-NC-ND license (<http://creativecommons.org/licenses/by-nc-nd/4.0/>).

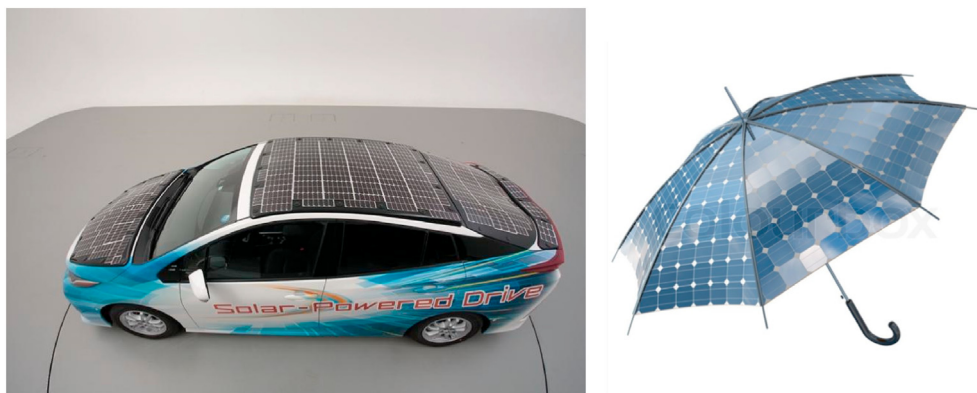


Fig. 1. The picture on the left is an electric car integrated with solar panels (photo courtesy of Toyota Canada Inc.). The picture on the right shows a concept umbrella made of flexible solar panels (photo courtesy of Colourbox.com).

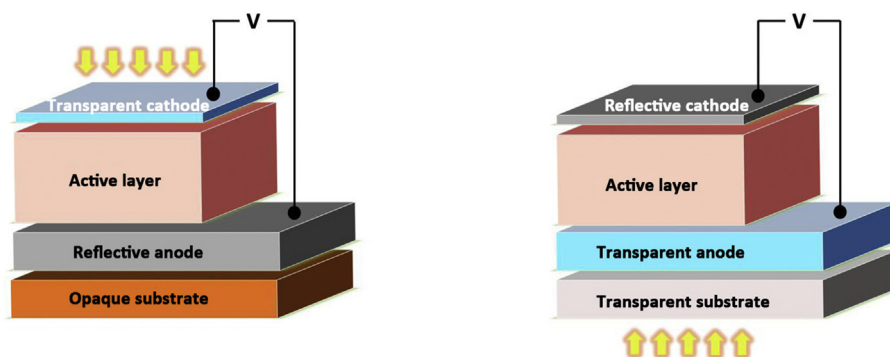


Fig. 2. Schematic structure of solar cells comprising various functional materials: a flexible substrate, two electrodes, and an active layer. The direction of light entry to the active layer determines the optical requirement for the substrate and the electrodes.

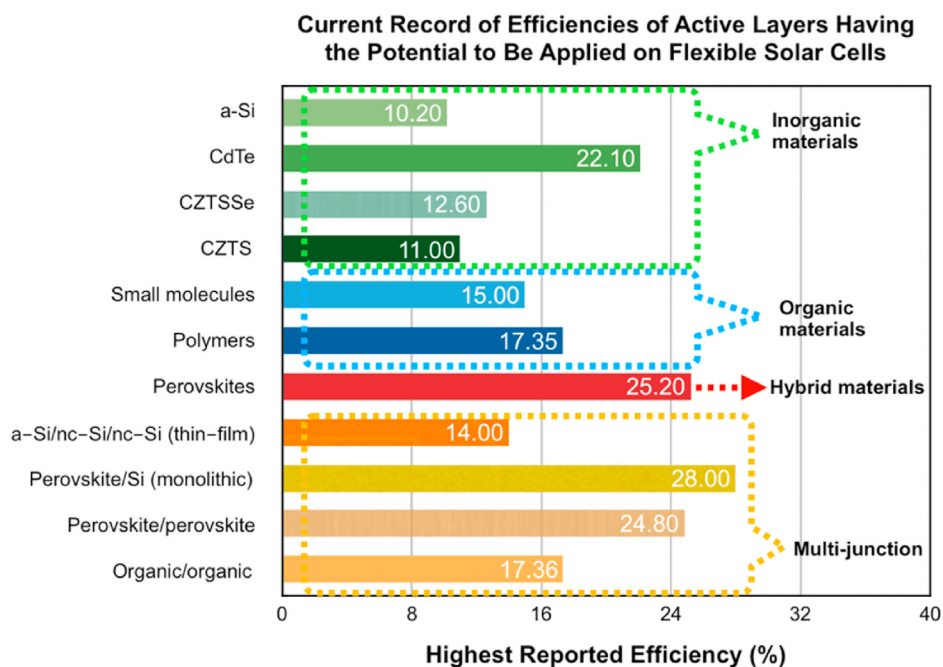


Fig. 3. Reported best efficiencies of solar cells made with various active materials. These active materials either have been made or have the potential to be made on flexible substrates.

in Fig. 2, which also illustrates the device structure on an opaque substrate (left) and a transparent substrate (right). In general, a thin-film solar cell is fabricated by depositing various functional layers on a

flexible substrate via techniques such as vacuum-phase deposition, solution-phase spin-coating, and printing. A flexible substrate provides mechanical support and environmental protection of the whole cell. Two

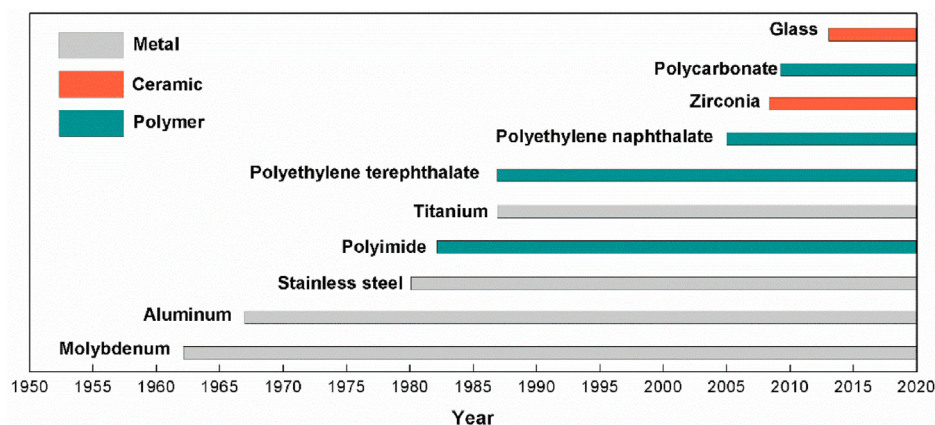


Fig. 4. Chronological chart of commonly used flexible solar cell substrates reported in literature.^{1–10}

electrodes collect photoelectric charge carriers as well as provide electrical leads to external circuits. One of the electrodes must be optically transparent allowing sunlight to enter the device to be absorbed by an active semiconductor layer which converts light to photoelectric charge carriers. As the key components of flexible solar cells, the active materials play a dominant role in power conversion efficiency. Active materials can be classified into three categories: inorganic, organic, and inorganic-organic hybrid semiconductors. Most common inorganic semiconductors are amorphous silicon, cadmium telluride and copper indium gallium diselenide. Organic semiconductors include donor and acceptor organic compounds, which are further classified by the size of molecules as small organic molecules and polymers. For inorganic-organic semiconductors, metal halide perovskite is the most promising material for flexible solar cells. Each class of active materials currently used in solar cells and potentially to be applied in the flexible form, along with the corresponding record certified efficiency, is presented in Fig. 3.

In this paper, we review recent progresses on various materials for manufacturing flexible solar cells. These materials include flexible substrate materials, active materials, and electrode materials. We also discuss technical requirements, current status and future R&D direction for each of these materials.

2. Substrates

Flexible substrate is one of the fundamental building blocks of flexible photovoltaics. Common flexible substrates for solar cell fabrication reported in literature,^{1–10} are shown in Fig. 4. They can be categorized according to the material they consist of, e.g., metal, ceramic, and plastic substrate. In the following sections, we will discuss merits, weakness and future perspectives for each class of substrate materials.

2.1. Metal substrate

Thin metal (<125 μm) foils are flexible and are often used as substrates to fabricate flexible solar cells.¹¹ High flexibility of metal foils rises from high ductility of metals. The most used flexible metal substrate is stainless-steel foil due to its low cost, excellent thermal and chemical stability. Its first reported use for solar cells (which could be flexible as well) can be traced back to 1980s, and the cases are hydrogenated amorphous silicon (a-Si:H) thin film solar cell and cadmium sulfide (CdS) based solar cell.^{3,12} The stainless-steel foil has now been applied to the commercial flexible solar panels, such as flexible copper indium gallium selenide (CIGS) solar panel manufactured by Global Solar company and GSHK company. In addition to the stainless-steel foil, aluminum alloy-foil has also been utilized as substrates of commercial flexible solar cells, exemplified by a product of Nanosolar company roll-to-roll printed on a low-cost aluminum-alloy foil. Other metals such as titanium (Ti) foil have

also been used in recent years for fabrication of perovskite solar cells (PSCs).^{13,14} A PSC with power conversion efficiency (PCE) of 13.07% has been achieved using a titanium dioxide nanowire array anode fabricated on the Ti-foil substrate.¹⁵ However, due to the high cost of the Ti-foil, the commercialization of this substrate may be unrealistic. It should be noted that metal foil has high optical reflectivity across the visible spectrum, and therefore the top electrode of the solar cell must be optically transparent allowing transmission of photons into the active materials.

2.2. Ceramic substrate

The most used ceramic substrate for solar cells is the glass substrate. Glass substrate shows good thermal stability and is resistant to chemical and moisture attacks. However, the poor ductility of glass compromises its flexibility, leading to a much smaller safe bending radius as compared with that of a metal foil or a plastic substrate.¹¹ With today's glass-making technology, the thickness of glass substrate can be thinned down below 100 μm , which makes the glass highly flexible. Willow® glass is a kind of flexible glass substrate manufactured by the Corning Company, which has been used by researchers to fabricate flexible solar cells. Starting from 2013, the flexible glass substrate has been used to fabricate flexible solar cell, etc.^{10,16–18} For example, a glass based flexible PSC with a PCE of 18.1% has been demonstrated by B. Dou et al., in 2017.¹⁷ In addition to glass substrate, other ceramic substrates like zirconia ribbon substrate have also been developed for solar cells.¹⁹ T. Todorov et al. reported a copper zinc tin sulfide-selenide (CZTSSe) solar cell fabricated by zirconia based flexible substrate which shows a PCE of 11.5%.²⁰

2.3. Plastic substrate

Plastic (or polymer) substrate has attracted great attentions in the field of flexible solar cells due to its light weight and low-cost. Recently, H. Yoon et al. demonstrated a perovskite solar cell (PSC) fabricated on a polyethylene naphthalate (PEN) substrate with a PCE up to 19.1%.²¹ The major drawback of a plastic substrate is its high permeability to oxygen and moisture which is detrimental to solar cells.^{22,23} This problem can be overcome by coating barrier layers on both sides of the plastic substrate. For example, aluminum oxide and silicon oxide are often coated on plastic substrate as barrier layers to prevent the permeation of the oxygen and moisture.^{22,24} Usually, a multi-layer coating is needed for the plastic substrate to satisfy the permeability requirement for an optoelectronic device. Another drawback of the plastic substrate is the low thermal stability due to its low glass transition temperature. Hence, the plastic substrate is not suitable for making solar cells that requires deposition of active semiconductor layers at elevated temperatures, for example, silicon solar cells or CIGS solar cells.^{25,26} However, the plastic substrate is

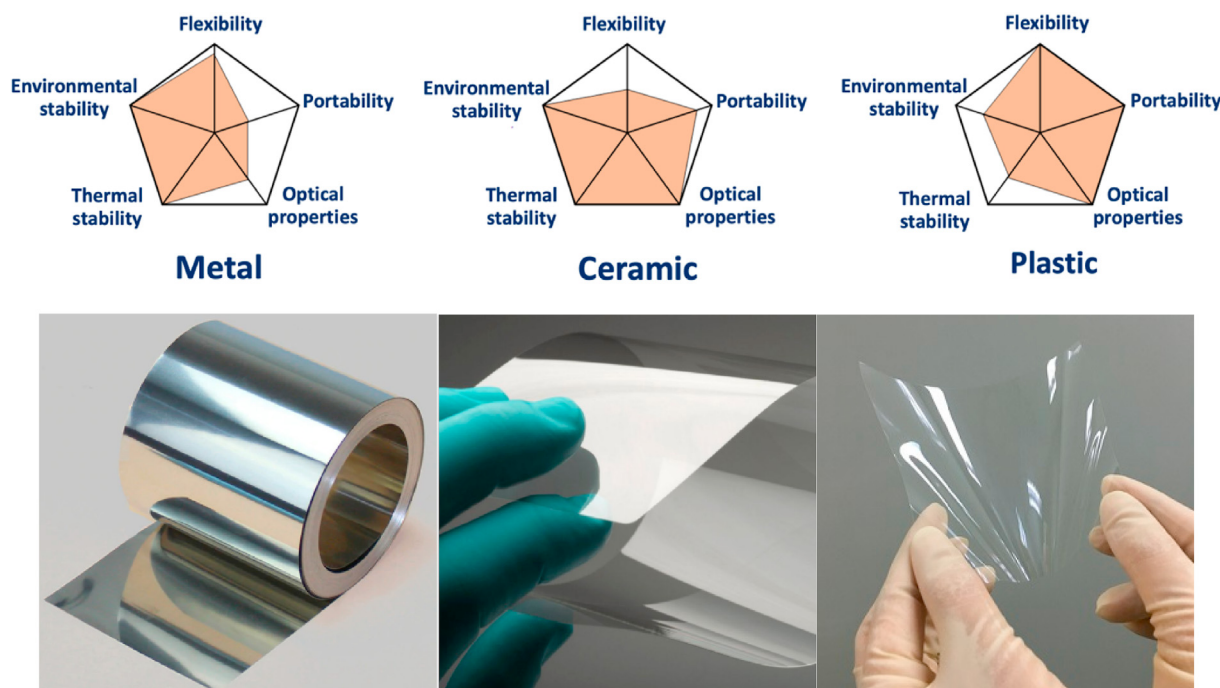


Fig. 5. Qualitative summary of five key materials properties of metal, ceramic, and plastic substrates. The bottom panel shows photographic picture of (left) stainless steel (source: <https://www.aliexpress.com/>), (middle) Corning willow glass (source: <https://www.corning.com/>), and (right) colorless polyimide (source: <http://www.koreaherald.com/>).

very suitable for solar cell fabrication at low process temperature such as organic/polymer solar cells and PSCs. Commonly used plastic substrates are polyethylene terephthalate (PET), PEN, polycarbonate (PC) and polyimide (PI).^{7,9,27,28}

2.4. Properties summary

Fig. 5 presents a qualitative comparison of different properties for metal, ceramic and plastic substrate used for solar cell fabrication. Some of these properties are briefly discussed as below.

2.4.1. Flexibility

Flexibility is the ability of material to be bended without mechanical failure such as fracture and plastic deformation. The definition of flexibility, though varied depending on manufacturers and users, generally involves the mechanical properties of part or all of the following capabilities: (1) bending or rolling without plastics deformation, (2) being permanently, shaped and (3) being stretched elastically.¹¹ The deformation of material can be divided into two categories: elastic deformation and plastic deformation. In general, when a load or stress is applied, the material initially undergoes an elastic deformation, which is a reversible process, until the applied load reaches the yield strength. And when the stress exceeds the yield strength, there will take place the plastic deformation which is no longer recoverable, and finally, material fracture with further increase of the applied load. Usually, ceramic material fractures before plastic deformation occurs and therefore ceramics are known to be non-ductile, i.e., brittle. The bendability and stretch ability of the material are determined by its characteristic of elastic deformation. The ability to be permanently shaped is determined by the characteristic of plastic deformation.

There are a few mechanical parameters describing the deformation of a material. For elastic deformation, Young's modulus and elastic elongation are two important parameters. Young's modulus is a measure of the stiffness of a material which is equal to the slope of stress-strain curve in the elastic deformation region. It describes a material's resistance to elastic deformation. Young's moduli of metals or ceramics are generally

much higher than that of polymers. For instance, 430 stainless-steel and soda-lime glass have a Young's modulus of ~ 190 GPa and ~ 70 GPa respectively, while the Young's modulus of PET is only ~ 3 GPa.^{29–31} Therefore, the bending and stretching of PET film is much easier. Another important parameter is the elastic elongation which is the maximum strain a material can endure while staying in the elastic deformation zone. It determines a degree of elastic deformation a material can reach. The elastic elongation is $\sim 10^{-3}$ for 430 stainless-steel and soda-lime glass, and $\sim 10^{-2}$ for PET.^{29,32,33} Therefore, PET is more flexible than the other two materials.

For plastic deformation, yield strength and total elongation are two key parameters. Yield strength refers to the stress at which the permanent deformation occurs, and total elongation is the total amount of strain before fracture. The former determines how resistant a material is to plastic deformation, and the latter describes the maximum degree of plastic deformation a material can reach. For instance, the yield strength for 430 stainless-steel and PET are ~ 200 MPa and ~ 40 MPa respectively,^{29,34} and, therefore, PET is easier to be permanently shaped. The total elongation is ~ 0.33 for 430 stainless-steel and ~ 0.70 for PET,^{31,35} indicating a much better formability of PET than 430 stainless-steel.

Thickness is also an important parameter for the substrate. The brittle ceramic material can also become very flexible when its thickness reduces under a few hundred micrometers, e.g., 100 μm for Corning® Willow® glass and 20 μm for Thin E-Strate® zirconia ribbon. The Young's modulus is ~ 70 GPa for soda-lime glass and ~ 200 GPa for zirconia.³⁶ Therefore, to reach the same flexibility, the substrate made of zirconia must be much thinner than that of soda-lime glass.

2.4.2. Oxygen and water vapor permeability

Oxygen and water vapor transmission rate (OTR and WVTR) are two important parameters to evaluate the oxygen and moisture permeability of materials. Depending on the application, the requirement for OTR and WVTR can be different. For example, the required OTR and WVTR of the substrate for organic solar cell are $10^{-3} \text{ cm}^3 \text{ m}^{-2} \text{ day}^{-1}$ and $10^{-3} \text{ gm}^{-2} \text{ day}^{-1}$, respectively.^{37,38} Metal and glass typically have extremely low OTR and WVTR because of the dense atomic packing of the materials.

Table 1

Summary of different substrates commonly used in flexible solar cells.

Material	Merits	Weakness	Future development
304 stainless steel ^{55–57}	<ul style="list-style-type: none"> - Cheap (~\$1.63/lb); - Good thermal stability; - Strength 655 MPa; - Ductile 55% elongation; - Impermeable to oxygen/moisture. 	<ul style="list-style-type: none"> - High surface roughness ~100 nm; - High coefficient of thermal expansion ~16.9 $\mu\text{m m}^{-1} \text{K}^{-1}$ at 20 °C; - Heavy (8.0 g cm⁻³). 	<ul style="list-style-type: none"> - Better surface polishing; - New low-cost method of depositing dielectric layer.
430 stainless steel ^{55,58,59}	<ul style="list-style-type: none"> - Cheap (~\$1.02/lb); - Resistance to oxidation; - Strength 483 MPa; - Low thermal expansion ~10.4 $\mu\text{m m}^{-1} \text{K}^{-1}$ at 20 °C; - Impermeable to oxygen/moisture. 	<ul style="list-style-type: none"> - High surface roughness ~70 nm; - Moderate ductility ~33% elongation at break; - Heavy (7.7 g cm⁻³). 	<ul style="list-style-type: none"> - Better surface polishing; - New low-cost method of depositing dielectric layer.
1050 Aluminum ^{60–64}	<ul style="list-style-type: none"> - Cheap (~\$1.56/lb); - Light (2.7 g cm⁻³); - Ductile ~40% elongation at break; - Impermeable to oxygen/moisture. 	<ul style="list-style-type: none"> - High surface roughness ~40 nm; - Low tensile strength ~75 MPa; - High thermal expansion ~21.8 $\mu\text{m m}^{-1} \text{K}^{-1}$; - Low working temperature ~200 °C. 	<ul style="list-style-type: none"> - Better surface polishing; - New low-cost method of depositing dielectric layer; - Application for low process temperature materials such as organic semiconductors.
CP-Titanium Grade 1 ^{60,65–67}	<ul style="list-style-type: none"> - Resistance up to 600 °C; - Strength up to 241 MPa; - Low thermal expansion ~8.6 $\mu\text{m m}^{-1} \text{K}^{-1}$ at 20 °C; - Impermeable to oxygen/moisture. 	<ul style="list-style-type: none"> - Expensive (~\$26.35/lb); - High surface roughness ~30 nm; - Low ductility ~24% elongation at break. 	<ul style="list-style-type: none"> - Better surface polishing; - New low-cost method of depositing dielectric layer; - Reduce cost.
Soda-lime Glass ^{68,69}	<ul style="list-style-type: none"> - Cheap (~\$0.60/lb); - Corrosive resistance; - Good thermal stability; - Low thermal expansion ~9.1 $\mu\text{m m}^{-1} \text{K}^{-1}$ at 20 °C; - Impermeable to oxygen/moisture. 	<ul style="list-style-type: none"> - Poor ductility ~0.05% elongation at break; - Low tensile strength ~35 MPa. 	<ul style="list-style-type: none"> - Reduce thickness and surface cracks to boost flexibility.
Zirconia ^{70–72}	<ul style="list-style-type: none"> - Corrosive resistance; - High thermal stability up to 1000 °C; - Low thermal expansion ~10.0 $\mu\text{m m}^{-1} \text{K}^{-1}$ at 20 °C; - Impermeable to oxygen/moisture. 	<ul style="list-style-type: none"> - Expensive (~\$12.00/lb); - Poor ductility ~0.15% elongation at break; - High surface roughness ~25 nm; - Heavy (5.7 g cm⁻³). 	<ul style="list-style-type: none"> - Reduce thickness to boost flexibility; - Reduce surface roughness.
PET ^{31,40,73–76}	<ul style="list-style-type: none"> - Cheap (~\$1.00/lb); - High ductility, up to 70% elongation at break; - Light (1.4 g cm⁻³). 	<ul style="list-style-type: none"> - Permeable to oxygen/moisture ~9 gm⁻² day⁻¹; - Poor thermal stability (T_g ~70 °C); - High coefficient of thermal expansion ~60 $\mu\text{m m}^{-1} \text{K}^{-1}$ at 20 °C; - Degradable under UV exposure. 	<ul style="list-style-type: none"> - Develop low-cost barrier coating technique.
PEN ^{40,75,77–79}	<ul style="list-style-type: none"> - High ductility up to 60% elongation at break; - Fair tensile strength ~200 MPa; - Light (1.4 g cm⁻³). 	<ul style="list-style-type: none"> - Expensive (~\$4.00/lb); - Permeable to oxygen/moisture ~2 gm⁻² day⁻¹; - High thermal expansion ~20 $\mu\text{m m}^{-1} \text{K}^{-1}$ at 20 °C; - Degradable under UV exposure. 	<ul style="list-style-type: none"> - Develop efficient and low-cost barrier coating technique.
PC ^{45,80–83}	<ul style="list-style-type: none"> - Cheap (~\$2.00/lb); - High ductility up to 70% elongation at break; - Light (1.2 g cm⁻³). 	<ul style="list-style-type: none"> - Degradable under UV exposure. - Permeable to oxygen/moisture ~50 gm⁻² day⁻¹; - High thermal expansion ~80 $\mu\text{m m}^{-1} \text{K}^{-1}$ at 20 °C; - Degradable under UV exposure. 	<ul style="list-style-type: none"> - Develop efficient and low-cost barrier coating technique.
PI ^{84–88}	<ul style="list-style-type: none"> - Good thermal stability (T_g ~350 °C); - Light (1.4 g cm⁻³). 	<ul style="list-style-type: none"> - Expensive (~\$50.00/lb); - Permeable to oxygen/moisture ~12 gm⁻² day⁻¹; - Low optical transparency; - High coefficient of thermal expansion ~30 $\mu\text{m m}^{-1} \text{K}^{-1}$ at 20 °C; - Degradable under UV exposure. 	<ul style="list-style-type: none"> - Develop efficient and low-cost barrier coating technique.

However, plastic materials usually have much higher OTR and WVTR, which is due to the loosely packed polymer chains leaving lots of voids inside the materials. The gas molecules or moisture vapor can permeate through these voids and can easily react with the active materials of the device. In addition, some polymers tend to absorb water while others do not. For instance, PC easily absorbs water vapor and a PC substrate with a thickness of 100 μm has a WVTR up to 50 gm⁻² day⁻¹, whereas PET is a hydrophobic polymer.³⁹ The WVTR of 100 μm thick PET substrate is 9 gm⁻² day⁻¹,⁴⁰ which still cannot meet the WVTR requirement for flexible solar cells. Therefore, elaborate layers of gas/moisture barrier coatings are crucial for the plastic substrate to function as a reliable substrate for advanced optoelectronic applications. The commonly used barrier coating materials are ceramics, such as silicon oxide (SiO_x), silicon nitride (SiN_x) and aluminum oxide (AlO_x). These materials have strong barriers to gas and moisture diffusion as well as high optical transparencies.⁴¹ However, a single barrier coating is usually inadequate for

device application. For example, the SiO_x coated PET substrate only shows a WVTR of ~10⁻¹ gm⁻² day⁻¹ and an OTR of ~10⁻¹ cm³ m⁻² day⁻¹.⁴² Multilayer organic/inorganic barrier stack is generally required to obtain satisfactory WVTR and OTR. For instance, the PET substrate coated with 5 stacks of AlO_x-polyacrylate pair shows a WVTR of ~10⁻⁵ gm⁻² day⁻¹.⁴³ Nevertheless, these multilayer coatings add substantial cost to the plastics substrates.

2.4.3. Thermal stability

Thermal stability is also an important factor of substrate materials, which determines whether the solar cell fabrication, employing the substrate, can be conducted at high temperature. Metals and ceramic glasses are tolerant of high temperature. For example, the stainless-steel is resistant to the temperature up to 900 °C and the glass can withstand the temperature up to 650 °C.¹¹ However, plastic materials usually have low thermal stability, limited by their glass transition temperature (T_g).

T_g is a critical temperature defining the transition between a rigid glassy network and a rubbery liquid-like state. Most plastics have low T_g , e.g., 70 °C for PET and 145 °C for PC.^{44,45} PI has a relatively high glass transition temperature of up to 300 °C,⁴⁶ which makes it the most used plastic substrate for making flexible devices including flexible AMOLED displays.

2.4.4. Environmental stability

The environmental stability of the substrate material is another important consideration for flexible solar cells. The substrate must be resistant to the environmental chemical attacks during outdoor solar cell operation. Metal based flexible substrates usually show good environmental stability. For example, stainless steel with high content of chromium (~10 wt%) can significantly resist the corrosion by acid and base.⁴⁷ Titanium is a reactive metal which can easily form a dense oxide layer once it is exposed to air. The formed passive oxide layer is able to prevent the further oxidation and make the titanium foil resistant to chemicals such as acid.⁴⁸ Ceramic materials also have a satisfactory environmental stability. Glass is chemically inert and is resistant to attacks by water, salt solutions, acids and organic substances. However, it cannot well withstand the attacks by base and hydrofluoric acid.⁴⁹ For the normal outdoor operation, the solar cells fabricated on metal foils or ceramic substrates can be environmentally stable. In contrast, plastic substrates show poorer environmental stability than metal or ceramic substrates since the easy degradation of polymers in the presence of environmental oxygen.⁵⁰ In addition, UV irradiation can make polymer very brittle.⁵¹ Therefore, UV filters are usually needed for protecting plastic substrates.

2.4.5. Optical properties

Optical properties of the flexible substrate should also be taken into serious consideration since they will determine how the solar cell structure should be designed. A substrate with either high optical transmittance or high reflectance is suitable for fabricating flexible solar cells. Optical transmittance and reflectance are two quantitative parameters defined as the ratio of transmitted light and reflected light over the total incident light, respectively. Stainless-steel shows a reflectance of 60%–70% over the visible spectrum and is not optically transparent.⁵² Glass-based substrate is optically transparent with an optical transmittance over 90%.⁴⁹ Flexible plastic substrate can also be very transparent. For instance, PET and PC exhibit optical transmittance of ~85% over the visible spectrum.^{7,53} Although PI is usually a partially transparent substrate with a poor transmittance within the blue region of the spectrum, it indeed can be made colorless nowadays via the novel molecular design.⁵⁴ For the solar cell fabricated on metal foil, the counter electrode must be transparent for the incident light transmitting into the photo-active material. However, for devices based on transparent glass or plastic substrates, the counter electrodes can be reflective or transparent depending on applications. The future window may be integrated with solar cell which requires excellent optical transparency of the substrate. The ceramic and plastic substrates will play significant roles in these types of applications.

2.5. Future development

Table 1 shows several examples of metals, ceramics and plastic materials and gives a detailed comparison between materials of each category. In the future, metal foil substrates, will still play a significant role in commercial flexible solar panel industry in making silicon and CIGS solar cells, due to its excellent flexibility and thermal stability. However, the metal foil usually has a high surface roughness which needs to be reduced through polishing to meet the requirement of electronics. The polishing process further increases the fabrication cost and, therefore, one future direction for metal foil based solar panel is to develop low-cost and efficient polishing process. In addition, the metal substrate is electrically conductive, and the monolithic integration of solar cell requires an

insulating layer between the substrate and electrode. Developing better deposition technique may further reduce the total cost of manufacturing. The flexible ceramic substrates have entered the market in recent years and its corresponding solar panels are now under commercial development. However, due to the brittle nature, the flexibility of ceramic substrate is still inferior to metal or plastic. Thus, the future effort for ceramic substrate should be placed on improving the flexibility by further reducing the thickness or developing new ceramic materials. The plastic substrate, such as PSC, allows solar cell fabrication at a low process temperature, and one future direction is to boost the efficiency and lifetime for these novel solar cells to the commercial level. However, as mentioned above, high gas/moisture permeability of plastic requires barrier coating on both sides, which further increases the manufacturing cost. Thus, another potential direction for plastic substrate is to develop cost-efficient coating technology. Lastly, a more efficient roll-to-roll manufacturing infrastructure is always required for lowering the product cost of flexible solar panels regardless of the substrate types.

3. Active semiconductor materials

In this section, we will discuss active materials used and potentially to be used in flexible solar cells. In general, if a photovoltaic material can be deposited onto a substrate at temperatures below 300 °C, the material can potentially be used in fabricating flexible solar cells. Several types of active materials, such as a-Si:H, CIGS, small organics, polymers, and perovskites, have broadly been investigated for flexible solar cell application. In the following sections, we will discuss the fundamentals of these materials and their strength, weaknesses, and future perspectives for flexible solar cells.

3.1. a-Si:H

Hydrogenated amorphous silicon (a-Si:H) has been used to fabricate efficient flexible solar cells.⁸⁹ The deposition of the a-Si:H film can be generally realized by plasma enhanced chemical vapor deposition (PECVD) and to a less degree chemical vapor deposition (CVD). The a-Si:H active materials possess a higher absorption threshold (700 nm) than that of crystalline silicon semiconductors (1107 nm)⁹⁰ and, thereby, leading to photon unharvested in the long-wavelength regime. In contrast to the crystalline counterparts where electronic states are extended Bloch wave, the a-Si:H exhibits a localized band states within films,⁹¹ as evidenced by relatively larger Urbach energies. The resulting device performance is inferior to those of crystalline Si solar cells. With the incorporation of hydrogen in the lattice, the deep trap states caused by dangling bonds are significantly reduced. Unfortunately, the presence of H leads to instability under sunlight illumination, known as Staebler-Wronski degradation. The mobility of a-Si:H is around 1 cm² V⁻¹ s⁻¹.⁹² And the transport joule losses within the thin film can be reduced by decreasing the thickness.

For a-Si:H-based flexible solar cells, a p-i-n configuration has broadly been utilized for generating and moving the charge carriers in which an intrinsic layer is attached to p- and n-type regions,⁹⁴ exhibiting a PCE of over 10%.⁹⁰ In the p-i-n devices, the a-Si:H layer absorbs most of the photons and produces electron-hole pairs. Subsequently, electrons migrate towards the n-type layer while holes migrate towards the p-type layer driven by the internal built-in electric field. Recent progress in making high-performance a-Si solar cells is employing the SiGe alloys in multijunction devices to form a-Si/a-SiGe/a-SiGe, which shows superior stability and respectable PCEs.⁹⁵ Similarly, triple-junction cells including all hydrogenated a-Si (a-Si:H), hydrogenated a-SiGe (a-SiGe:H), and hydrogenated nanocrystalline Si (n-Si:H) layers have also been explored. Very recently, the Hanenergy group, a renewable energy company focusing on thin-film solar cell technologies, has announced Si-based flexible heterojunction solar cells with a recorded efficiency of 23.61%. Fig. 6 (b) shows a picture of this type of Si heterojunction flexible cells.

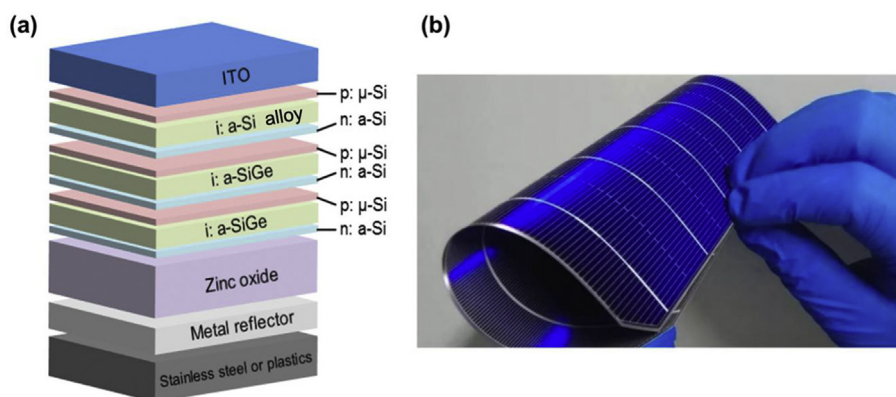


Fig. 6. (a) Illustration of a flexible triple-junction silicon solar cell, where μ -Si is microcrystalline silicon,⁹³ p: μ -Si, n: a-Si, i: a-SiGe/a-Si alloy. (b) A photograph of a silicon-heterojunction solar cell with excellent bending capability (courtesy of Hanenergy group, China).

3.2. CIGS

Compared with a-Si:H, Cu(In,Ga)Se (CIGS) materials have fewer defects within a solid film and are equally attractive for flexible photovoltaic applications. **CIGS-based materials have rapidly moved to the forefront of flexible solar cells.** By adjusting the gallium content, a bandgap exceeding 1.50 eV is achievable, although most CIGS bandgaps are between 1.25 and 1.45 eV⁹⁶. There are several approaches for CIGS preparation,⁹⁷ including evaporation, sputtering, solution processing, etc. To obtain high-quality CIGS films, the CIGS layer can be either manufactured by a single step with co-evaporation or crystallized by sequential metal stacking.⁹⁸ The best-performing CIGS flexible solar cells are made by vacuum co-deposition, which allows facile tuning of the chemical composition and thickness of the CIGS layer. This enables graded bandgap structures to facilitate photo-carrier transport and achieve high energy conversion. To date, a vast majority of works have confirmed that highly efficient flexible CIGS solar cells can be obtained by sputtering deposition and selenization-based process.⁹⁹ To further improve the device performance, various passivation strategies have employed to reduce the defects in CIGS solar cells. For example, incorporation of alkali elements (sodium, potassium, and cesium) has been extensively exploited for defect passivation of the CIGS layer.¹⁰⁰ With the defects passivation by introducing potassium, a record efficiency of 22.6% has been reported.¹⁰¹

3.3. Organic semiconductors

In addition to flexible substrates, interface buffer layer and morphology optimization of the photoactive layer composed of a p-type organic semiconductor donor and an n-type organic semiconductor acceptor also play crucial roles in improving the photovoltaic

performance of the flexible organic solar cells (OSC).^{102–105} The photocurrent and photovoltage generation, the conversion process from photons to electrons and holes in the active materials, can be divided into four key steps.^{106,107} Step (1), photoactive layer absorbs photons to generate bound electron-hole pairs referred to as excitons. Step (2), excitons diffuse towards the donor/acceptor interface. Before reaching the interface, some excitons will be lost due to exciton recombination. Step (3), exciton will dissociate into free holes and electrons at the interfaces, depending on the energy offset.¹⁰⁸ Step (4), electrodes harvest holes and electrons.

A typical OPV device is manufactured by sequential deposition on a flexible transparent electrode of a hole-transporting layer, a photoactive layer, an electron-transporting layer, and a metal cathode. For example, poly(3,4-ethylenedioxythiophene): poly(styrenesulfonate) (PEDOT: PSS) bilayer is used to harvest holes, and LiF/Al or Ca/Al bilayer serves as the top cathode to harvest electrons. The low work function (WF) metal such as Al is susceptible to oxidation under ambient conditions, resulting in device degradation.¹⁰⁹ Thus, the conventional OPV devices are prone to moisture attack. Inverted structure is another type of OPV.^{110,111} In an inverted structure, the bottom transparent electrode serves as the cathode whereas the top high WF electrode works as the anode. N-type low WF metal oxides (like ZnO or TiO₂) are usually inserted between the bottom cathode and organic active layer as the electron transport layer (ETL) to collect electrons. High WF metal oxides (such as MoO₃, WO₃, or NiO_x) serve as the hole transport layer (HTL) between the active layer and the top anode to collect holes.¹¹² The polarity of charge collection is reversed in the inverted structure compared to that of the conventional structure. In the inverted devices, the reliable air stability of the top anode made by high WF metals like Au or Ag favors the device stability. Particularly, the metal oxide transporting layers can be deposited from colloidal solution, which is suitable for an all-solution roll-to-roll

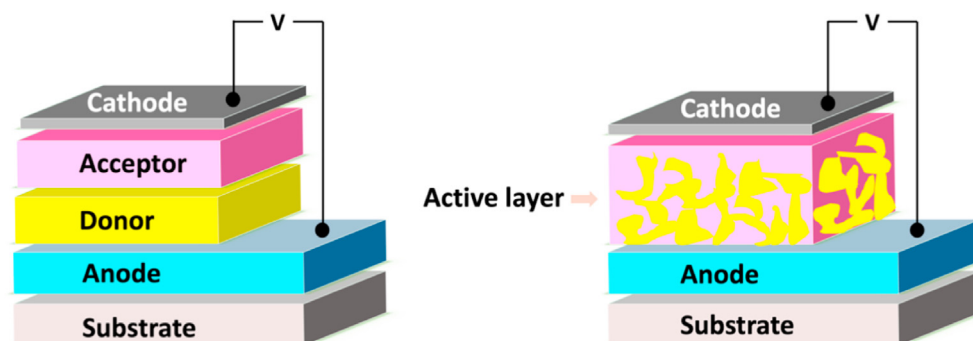


Fig. 7. Two distinct device architectures, donor/acceptor planar heterojunction (left) and donor/acceptor bulk heterojunction (right), commonly used to fabricate organic solar cells.

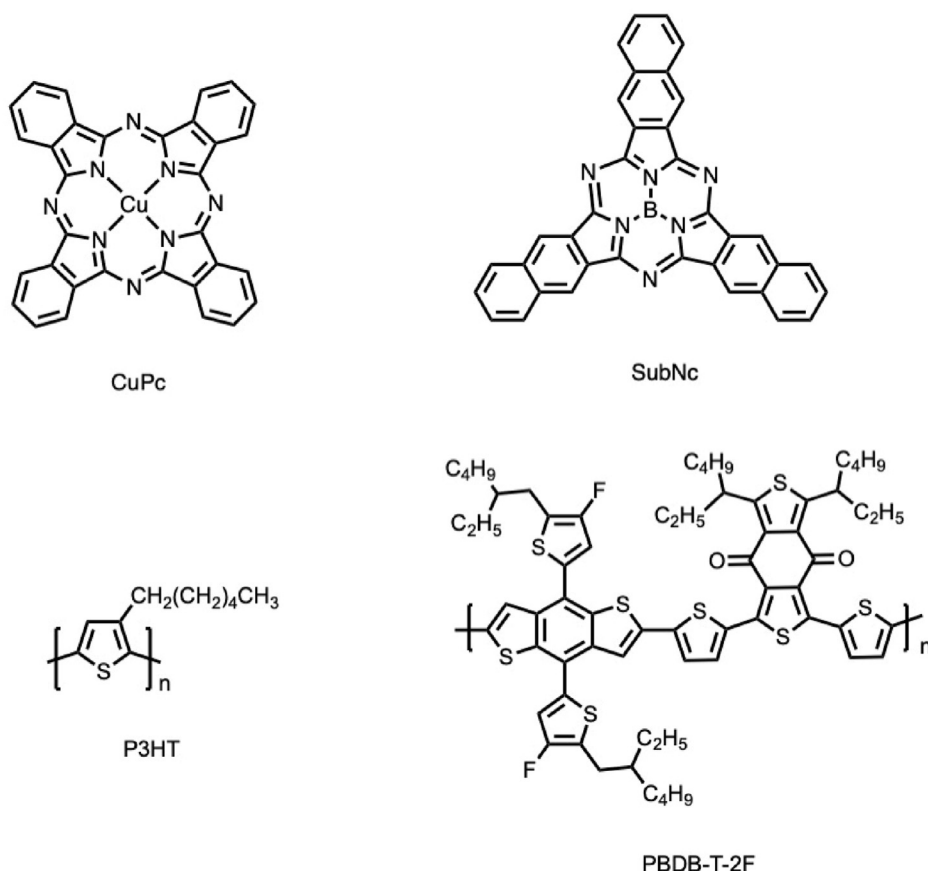


Fig. 8. Chemical structures of selected donor molecules.

processing technology.^{113,114}

In the active layer, there are also diverse types of donor-acceptor interface structures (Fig. 7). The simple bilayer planar heterojunction cells are made via sandwiching two layers of organic electronic materials between two metallic conductors. To enhance the interface area for photocarrier production, another type of cell called bulk heterojunction cell with interpenetrating group of donor and acceptor materials is invented.¹¹⁵ In a bulk heterojunction, a phase-aggregated donor/-acceptor blend forms the donor and acceptor domain having sizes closely matching the exciton diffusion length. The excitons generated in either of the materials may reach the D-A interface more readily.

3.3.1. Light absorption

Historically, poly(3-hexylthiophene-2,5-diyl) (P3HT) donor has been applied to capture light. However, P3HT can harvest merely ~20% of the sun light due to its wide bandgap (650 nm). Substantial efforts have been devoted to developing new materials that can harvest photons at longer wavelengths. Fluorene copolymers^{116–118} synthesized by enhancing strength of the internal acceptor in D-A-D fragment¹¹⁹ have been found to have narrow bandgap resulting in high PCE.^{120,121} Thus, narrow bandgap OPV materials are important for photon harvesting.¹²² A narrow bandgap (<2 eV) polymer absorbs light with wavelengths longer than 620 nm, which lead to higher photovoltaic performance.¹²³ In addition, a narrow bandgap acceptor with higher LUMO (lowest unoccupied molecular orbital) will also bring about the enhancement of the open circuit voltage (V_{oc}) and PCE.¹²⁴ Introducing conjugated dyes into absorbers helps light harvesting as well. For example, 9,10-diphenylanthracene (DPA) was studied for its effect on the performance of OPV with various doped concentrations.¹²⁵ Adding 2.6 mg of DPA into P3HT:PCBM blend increased short circuit current from 3.4 to 4.12 mA cm⁻². For the same reason, the fill factor (FF) and PCE were improved by adding 6 mg of the

dye, increasing from 0.35 to 0.66% to 0.5 and 1.09%, respectively.

Device structure engineering can also be an effective approach to improve the absorption efficiency. For instance, Rand et al. have introduced an ultrathin tin-phthalocyanine (SnPc) molecular layer between copper (II) phthalocyanine (CuPc) and C₆₀ films. As the SnPc layer has a very high absorption coefficient which extends to 1000 nm, this development represents an important step toward achieving OPVs with absorption in the near infrared segment.¹²⁶

3.3.2. Exciton diffusion

The typical singlet exciton diffusion length in polymeric materials is ~10 nm.^{127–129} Thus, if the thickness of active layer is within the exciton diffusion distance, more photo excitons can arrive at the interface and then dissociate into free charge carriers. However, in actual devices the thickness of active layer usually exceeds 10 nm for the sake of absorbing enough light. As a result, the PCEs of simple bilayer structures are low because their D-A interface are beyond the diffusion range of some excitons.¹³⁰ Rand et al. demonstrated a method of increasing the exciton diffusion length of a fluorescent donor layer through the process of sensitized phosphorescence. The generated singlet excitons can be transferred into triplet excitons by a properly matched dopant medium. The phosphorescent molecule platinum octa-ethyl porphyrin doped poly(phenylene vinylene) host, with an optimized doping concentration of 5 wt%, could bring about the increase of exciton diffusion length from (4 ± 1) to (9 ± 1) nm. Thanks to increased exciton diffusion length, photocurrent from the doped layer in OPV devices boosted 40%.^{131,132} Instead of using the new molecules to enlarge exciton diffusion lengths, many researchers have been devoted to shortening the distance between donor and acceptor molecules.^{133–135} In a single heterojunction solar cell, direct contact between the deposited electrode and organic active layer can lead to exciton quenching. A device architecture with stacking of two

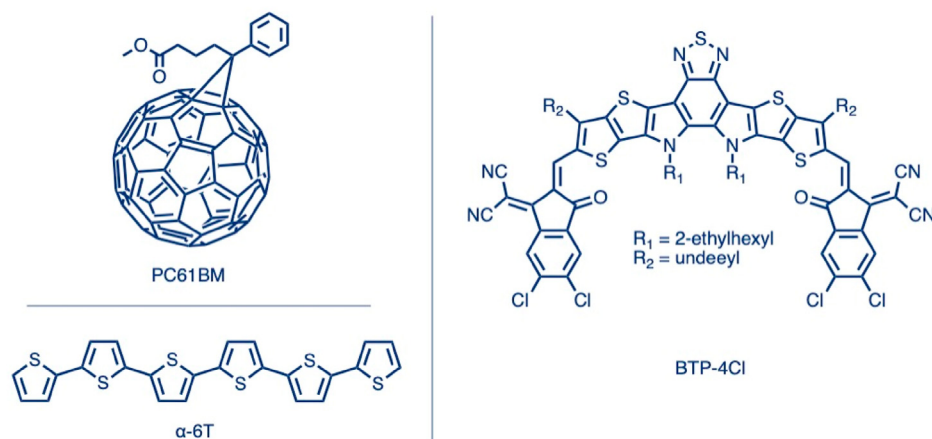


Fig. 9. Chemical structures of selected acceptor molecules.

Table 2

Summary of small molecule-based donor/acceptor heterojunction cells.

Active materials (donor/acceptor)	Merits	Weakness	Future development
Metal-Pc/C60	PVD deposition can be easily scaled up for mass production. CuPc and C60 are stable and cheap.	Poor light harvesting.	Tandem cells.
Metal-Pc/C70	PVD deposition can be easily scaled up for mass production.	C70 is expensive. Poor light harvesting.	Tandem cells.
Metal-Pc/PCBM	PCBM has high electron mobility and good solubility.	PCBM is expensive. Poor light harvesting.	Tandem cells.
DPP/PCBM	PCBM has high electron mobility and good solubility.	PCBM is expensive. Poor light harvesting.	Tandem cells.
Squaraine/PCBM	Fair light harvesting.	PCBM is expensive.	>10% tandem cells.
DTS(PTTh) ₂ /PCBM	Fair light harvesting.	High materials cost.	>12% tandem cells.
(p-DTS(FBTTh) ₂)/PCBM	Good light harvesting.	High materials cost.	>15% tandem cells.
DRTB-T: IC-C6IDT-IC	Good light harvesting.	Low electron mobility. Low open circuit voltage.	>10% single junction cell. >18% tandem cells.
BIT4F/PCBM	Good light harvesting.	High materials cost.	>10% single junction cell. >18% tandem cells.
DTBDT-based (ZR1): IDIC-4Cl	ZR1 has broad absorption. Non-fullerene acceptor.	Low electron mobility. Low open circuit voltage.	>10% single junction cell. >19% tandem cells.
ZnP-TBO: 6TIC	Excellent light harvesting.	Low open circuit voltage.	>13% single junction cell. >20% tandem cells.
DTBDT-based (ZR1): Y6	Excellent light harvesting. ZR1 has broad absorption. Non-fullerene acceptor.	Low electron mobility. Low open circuit voltage.	>16% single junction cell. >25% tandem cells.

single heterojunctions, which is also called a double heterojunction device, can effectively confine the generated excitons within the photo-active layer, giving rise to a higher internal efficiencies.¹²⁸ Recently, Burlingame et al. demonstrated a multilayer structure, in which the electrically and optically generated electrons are able to be effectively confined to a single organic layer (a thin fullerene channel) and diffuse over very long distances.¹³⁶

3.3.3. Flexible OPVs with small molecules/polymers

As mentioned above, the active layers are generally composed of p-type organic semiconductor donor and n-type organic semiconductor acceptor. The chemical structures of the most commonly used donor molecules and acceptor molecules are shown in Fig. 8 and Fig. 9, respectively. The p-type electron donors include small molecules and conjugated polymers. The n-type electron acceptors are a series of fullerene derivatives and non-fullerene molecules. To efficiently harvest a broad range of photons, the absorption spectra of the active layer should well match with the sun light spectrum from the visible to near-infrared region. The V_{oc} in the bulk heterojunction OSC is related to the energy level difference between the HOMO of the donor and the LUMO of the acceptor.^{108,137,138}

In addition to the bandgap and energy levels, ideal morphology also contributes to charge separation and transport, high and balanced hole/electron carrier mobility, and good miscibility between donor and acceptor molecules, which should also be taken into consideration for high-performance OPVs. During the past decades, a great number of donors and acceptors have been designed and synthesized. In Tables 2 and 3, we provide a summary of various materials, D/A structures and their merits, weakness, and future perspective. In Table 4, we provide a historical development of device performance from 1975 to 2020.

3.4. Perovskite active materials

Metal halide perovskites can be prepared via a low-temperature process to form direct-bandgap crystalline materials with outstanding optoelectronic properties. Typical metal halide perovskites bear a three-dimensional (3D) crystal structure, with a general formula of ABX_3 (Fig. 10 (a)), where A is a monovalent cation (e.g., FA^+ = formamidinium, MA^+ = methylammonium, or Cs^+), B is a divalent metal cation (e.g., Pb^{2+} or Sn^{2+}), and X is a halogen anion (e.g., I^- , Br^- , or Cl^-). Their crystallographic stability and probable structure are governed by the Goldschmidt tolerance factor (t) and octahedral factor (v): t is defined by a relation of $(R_A + R_B)/\sqrt{2}(R_B + R_X)$, where R_A , R_B , and R_X are the ionic radii of the corresponding ions; and v is defined as R_B/R_X . To realize

Table 3
Summary of polymer-based donor/acceptor heterojunction solar cells.

Active Materials (donor/acceptor)	Merits	Weakness	Future development
P3HT/PCBM	Material savings by solution casting.	Poor light harvesting.	>6% BHJ cell
PBDTBD/PCBM	Material savings by solution casting.	Poor light harvesting.	>8% BHJ cell
PCPDTBT/PCBM	Material savings by solution casting.	Poor light harvesting.	>8% BHJ cell
PCDTBT/PCBM	Material savings by solution casting.	Poor light harvesting.	>9% BHJ cell
F-PCPDTBT/PCBM	Material savings by solution casting.	Poor light harvesting.	>9% BHJ cell
PDTP-DFBT/PCBM	Material savings by solution casting. Good light harvesting.	PCBM is expensive.	>10% BHJ cell
PPDT2FBT/PCBM	Material savings by solution casting. Good light harvesting.	PCBM is expensive.	>11% BHJ cell
PTB7/PCBM	Material savings by solution casting. Good light harvesting.	PCBM is expensive.	>11% BHJ cell
PBDTTT-C-T/PCBM	Material savings by solution casting. Good light harvesting.	PCBM is expensive.	>11% BHJ cell
PBDT-TS1/PCBM	Material savings by solution casting. Good light harvesting.	PCBM is expensive.	>12% BHJ cell
PTB7-Th/PCBM	Material savings by solution casting. Good light harvesting.	PCBM is expensive.	>12% BHJ cell
PTB7-Th/ITIC	Material savings by solution casting. Good light harvesting.	Poor light harvesting.	>9% BHJ cell
PDBT-T1/SdiPBI-S	Material savings by solution casting.	Poor light harvesting.	>9% BHJ cell
PTB7-Th/hPDI4	Material savings by solution casting. Good light harvesting.	Poor photochemical stability.	>10% BHJ cell
PDBT-T1/ITIC-Th	Material savings by	Poor photochemical stability.	>12% BHJ cell

Table 3 (continued)

Active Materials (donor/acceptor)	Merits	Weakness	Future development
PBDB-T/ITIC	solution casting. Good light harvesting. Material savings by solution casting. Good light harvesting.	Complex molecular structures and verbose synthesis. Toxic halogenated solvents. Poor photochemical stability.	>13% BHJ cell
PBDB-T/IT-M	Material savings by solution casting. Excellent light harvesting.	Complex molecular structure and verbose synthesis. Toxic halogenated solvents. Poor photochemical stability.	>15% BHJ cell
PBDB-T-SF/IT-4F	Material savings by solution casting. Excellent light harvesting.	Complex molecular structures and verbose synthesis. Toxic halogenated solvents. Poor photochemical stability.	>15% BHJ cell
DTDCPB:PCBM/PTB7-Th/BT-CIC	Material savings by solution casting. Excellent light harvesting.	Complex molecular structure and verbose synthesis. Toxic halogenated solvents. Poor photochemical stability.	>17% BHJ cell
PDDB-T:F-M/PTB7-Th:O6F-4F:PCBM	Material savings by solution casting. Excellent light harvesting.	Complex molecular structures and verbose synthesis routes. Toxic halogenated solvents. Poor photochemical stability.	>19% BHJ cell

3D perovskites, t and v are expected to be in the range of $0.81 < t < 1.11$ and $0.44 < v < 0.90$, respectively. Otherwise, they usually arrange into the Ruddlesden–Popper phase ($R_2A_{n-1}B_nX_{3n+1}$), i.e., 2D or quasi-2D perovskites, where the size of the organic bulky cation (R) exceeds the limitation of the Goldschmidt tolerance factor, and n is the number of the octahedra layers in perovskites.

The first attempt to use perovskite as active material in flexible solar cells can be tracked to 2013,¹⁸⁵ and an initial efficiency of $\sim 2.6\%$ was reported (Fig. 10 (b)). Acting as active materials in flexible solar cells, perovskite exhibits several exceptional benefits. Specifically speaking, the tunable bandgap of perovskites used in solar cells can be further engineered by utilizing mixed ions at the A, B, and X sites,¹⁸⁶ in the range of 1.24–3.55 eV (Fig. 10 (c)), among which the perovskite with a narrow bandgap (< 1.65 eV) is appropriate for single-junction devices, and perovskites with a slightly wider bandgap in the range of 1.70–1.80 eV have been proved to be suitable for a top sub-cell of multifunction devices. Perovskite is a direct bandgap semiconductor, with the light absorption coefficients on the order of up to $\sim 10^5 \text{ cm}^{-1}$.¹⁸⁷ Perovskite active materials possess a low Urbach energy of 14 meV, which is comparable to other direct bandgap absorbers (e.g., GaAs).¹⁸⁷ Meanwhile, the carrier mobility of perovskite active materials, $\sim 10\text{--}30 \text{ cm}^2 \text{ V}^{-1} \text{ s}^{-1}$, is much higher than that of most organic semiconductors and is approximately ten times higher than the a-Si:H.

Presently, all efficient perovskite solar cells comprise an intrinsic perovskite absorber (i) sandwiched between positive (p)- and negative (n)- charge extraction layers, which are termed as p- and n-type interfaces, respectively. The PSCs are generally classified into three categories: mesoporous n-i-p, planar n-i-p, and planar p-i-n devices.¹⁹² The regular n-i-p configurations have been evolving from dye-sensitized solar cells, while the p-i-n configurations (also known as inverted structure)

Table 4

Evolution of small organic and polymer solar cells.

Year	Donor	Acceptor	PCE	Area (cm ²)	Substrate	Thickness (μm)
1975 ¹³⁹	Chl-a	metal	0.001%	0.5	Glass	
1986 ¹⁴⁰	CuPc	PV	1%		Glass	
2004 ¹⁴¹	MDMO-PPV	PC ₆₁ BM	3.00%	0.25	PET	175
2007 ¹⁴²	P3HT	PC ₆₁ BM	1.5%	17.1	PET	175
2007 ¹⁴³	PCPDTBT	PC ₇₁ BM	5.5%		Glass	
2009 ¹⁴⁴	P3HT	PC ₆₁ BM	3.73%	0.046	PES	200
2010 ¹⁴⁵	P3HT	PC ₆₁ BM	4.18%	0.04	PEN	
2011 ¹⁴⁶	DTS(PTTh ₂) ₂	PC71BM	6.7%	0.196	Glass	
2011 ¹⁴⁷	squaraine (SQ)	PC71BM	5.2%	0.008	Glass	
2012 ¹⁴⁸	DTS(FBTTh ₂) ₂	PC71BM	7.0%		Glass	
2013 ¹⁴⁹	p-DTS(FBTTh ₂) ₂	PC71BM	7.88%		Glass	
2014 ¹⁵⁰	PIDTT-DFBT	PC ₇₁ BM	10.2%	0.045	PET	
2014 ¹⁵¹	PTB7	PC ₇₁ BM	8.71%	0.16	PET	125
2014 ¹⁵²	SubNc	α-6T	8.4%		Glass	
2014 ¹⁵³	DRCN7T	PC ₇₁ BM	9.3%		Glass	
2014 ¹⁵⁴	PBDTTT-C	PC ₇₁ BM	5.55%		PET	–
2014 ¹⁵⁵	PIDT-PhanQ	PC ₇₁ BM	6.04%		PEN	–
2015 ¹⁵⁶	PBTZT-stat-BDIT-8	Merck PV-A600	6.50%	0.27	PET	
2015 ¹⁵⁷	P2 (synthesized)	PC ₇₁ BM	7.42%	0.15	cPI	20
2015 ¹⁵⁸	PTB7-Th	ITIC	6.8%		Glass	
2015 ¹⁵⁹	PTB7-Th	Hpdi4	8.3%		Glass	
2015 ¹⁶⁰	PBDTT-F-TT	PC ₇₁ BM	10.4%	1	PET	
2015 ¹⁶¹	PTB7-Th	PC ₇₁ BM	9.9%	0.0464	PEN	125
2015 ¹⁶²	DRCN5T	PC ₇₁ BM	10.1%		Glass	
2016 ¹⁶³	DCV5T-Me	PC ₆₁ BM	7.84%		Glass	217
2016 ¹⁶⁴	PDBT-T1	ITIC-Th	9.6%		Glass	
2016 ¹⁶⁵	PDBT-T	IT-M	12.05%		Glass	
2016 ¹⁶⁶	BIT6F	PC ₇₁ BM	9.1%	0.032	Glass	
2017 ¹⁶⁷	DRTB-T	IC-C6IDT-IC	9.08%		Glass	
2017 ¹⁶⁸	PBDB-T-SF	IT-4F	13.1%		Glass	
2017 ¹⁶⁹	H11 with bithienylbenzodithiophene (BDTT)	IDIC	9.73%		Glass	
2017 ¹⁷⁰	SM1	IDIC	10.11%		Glass	
2017 ¹⁷¹	PTB7-Th	PC ₇₁ BM	8.6%	0.04	Glass	
2018 ¹⁷²	PTB7-Th	PC ₇₁ BM	10.04%	0.1	PET	
2018 ¹⁷³	PBDTTT-OFT	PC ₇₁ BM	10.49%	0.04	Parylene	1
2018 ¹⁷⁴	PBDTTT-OFT	PC ₇₁ BM	10.00%	0.04	cPI	1.3
2018 ¹⁷⁵	PTB7-Th CO8DFIC	PC ₇₁ BM	14.62%		Glass	
2018 ¹⁷⁶	PBDB-T-2Cl	IT-4F	14.4%	0.03774	Glass	
2018 ¹⁶⁹	PDTB-EF-T	IT-4F	14.2%		Glass	
2019 ¹⁷⁷	PTB7-Th	3 TT-FIC	12.1%		PET	
2019 ¹⁷⁸	PM6: Y6	PC ₇₁ BM	14.06%		PET	
2019 ¹⁷⁹	PBDB-TF	IT-4F	15.1%		Glass	
2019 ¹⁸⁰	DTBDT-based (ZR1)	Y6	14.34%		Glass	
2019 ¹⁸¹	PM6	Y6	15.7%	0.05	Glass	
2019 ¹⁸²	PBDB-TF	BTP-4Cl	15.3%	1.0	Glass	
2019 ¹⁸²	PBDB-TF	BTP-4Cl	16.5%	0.09	Glass	
2020 ¹⁸³	PBDB-T-2F	Y6	15.21%		PET	
2020 ¹⁸⁴	D18	DTBT	18.22%		Glass	

are the same as the organic solar cells. Both configurations are compatible with flexible substrates and can be applied in flexible solar cells. Under sunlight illumination, the perovskite active material absorbs incident photons with energies (greater than bandgaps) to generate electron-hole pairs. Photogenerated electron-hole pairs in perovskites have binding energies much less than room-temperature thermal energy, free charge carriers are formed almost instantaneously. These photogenerated holes and electrons will freely move to respective electrodes prior to recombination if trap states are sufficiently low, and, thereby, realizing the conversion of light to electricity (Fig. 11). In a practical solar cell, there are several undesirable processes causing losses in energy conversion efficiency. These losses include optical losses and electrical losses. To minimize the unwanted optical losses, researchers have developed some strategies,¹⁹³ such as using high transmittance semi-transparent electrodes and substrates, adding an anti-reflection layer comprised of magnesium fluoride. To reduce electrical losses, defect passivation and crystallization have been controlled commonly. Upon successful reduction of undesirable losses, certified PCE has reached 25.2%, which is already comparable to traditional solar cells, such as crystalline Si and CIGS cells.

As mentioned earlier, a sharp increase in PCEs for flexible PSCs has

been achieved in the past few years.¹⁹⁴ We attribute these notable advancements in device performances to their excellent optoelectronic properties and to lessons learned from organic solar cells and dye-sensitized solar cells. By combining chemically stable oxides with inverted device structure, flexible PSC with a triple-cation composition exhibited a PCE of 18.6%, with a highly stabilized power output of 17.7% at the maximum point.¹⁹⁵ Through ligand-free and highly crystalline oxide transport layer, the flexible PSC achieved a certified PCE of 17.3%.¹⁹⁶ Recent works have also demonstrated that flexible all-perovskite tandem solar cells have enabled high device efficiencies, reaching 21.3%.¹⁹⁷ In addition, in coordination with the demand for foldable cells, two types of folding modes: in-folding and out-folding have been created. The in-folding mode requires an extremely small bending radius of curvature like 2 mm, which is a great challenging in cells comprising inorganic semiconductors, such as Si. Flexible perovskite solar cells adopting PFN substrates showed 1000 times bending durability at the radius of curvature of 4 mm,¹⁹⁸ and over 86% of the stabilized power output is retained after 1000 h aging. The device constructed on a 57-mm-thick PET-based substrate has demonstrated excellent robustness against mechanical deformation, retaining 95% of its original efficiency after 5000 times of cyclic bending.¹⁹⁹

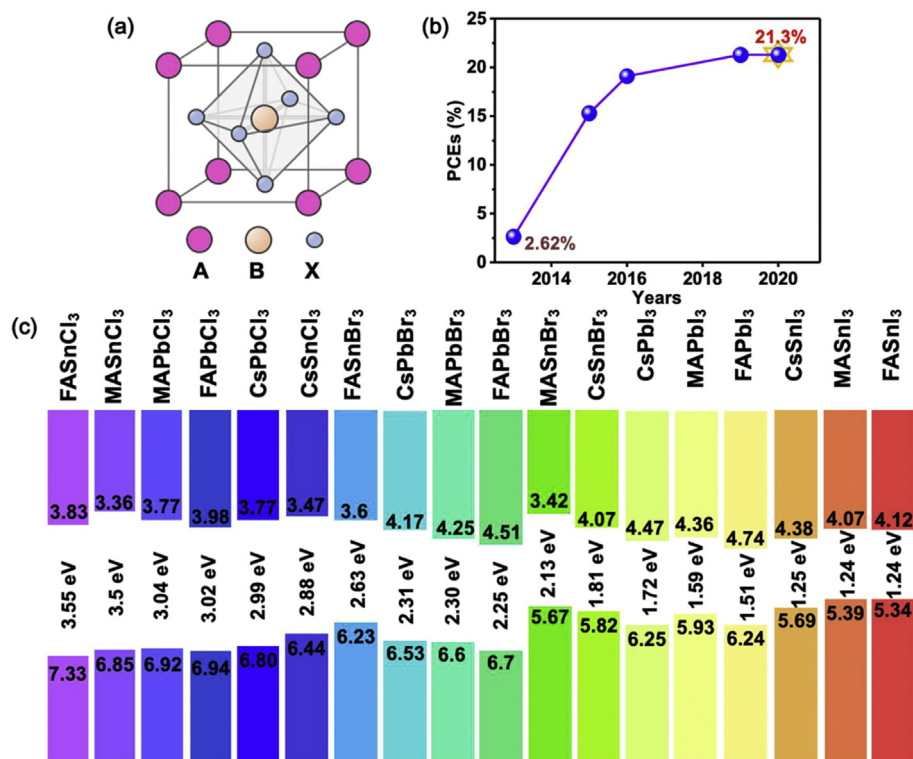


Fig. 10. (a) Crystal structure of metal halide perovskites with an ABX₃ structure. (b) Summary of recent advances in PCEs of flexible perovskite solar cells.^{188–190} (c) Schematics of energy levels for various metal halide perovskites.¹⁹¹

Despite remarkable improvements in PCEs, long-term stability suitable to deliver greater than 25 years of outdoor operation remains to be proven. One concern is that the state-of-art perovskites have multiple compositions within a film, and the exposure of perovskites to light leads to substantial degradation. Typically, light soaking can trigger ion migration throughout the thin film, resulting in reduced device stability.¹⁸⁷ And light soaking can also accelerate the redistribution of halogen ions over the film.²⁰⁰ The device degradation upon thermal stress may arise from the deterioration of materials and interfaces.¹⁹² Hence, a pressing issue is to address the operational stability of flexible perovskite solar cells under thermal and light stresses. To stabilize the nature of perovskite active materials and related interfaces, it is feasible to tune the quality of the thin film simply by modifying the chemical compositions.²⁰⁰ Following this logic flow, flexible solar cells based on the interface optimizations have already shown improved stability in air.²⁰¹

In addition to device stability, the relatively low absorption in near-infrared region and the toxicity of lead are increasingly problematic at

present. To date, ternary organic active materials as charge transport layers in the flexible perovskite solar cells are alternative to simultaneously enhance mechanical flexibility and extend the absorption threshold for single-junction devices. This three-component transporting layer with a wide absorption window can be easily obtained without multiple stacking.²⁰² Through a rational selection of organic semiconductors that are readily accessible in the market, the integrated solar cells containing both the perovskite and organic active materials show huge potentials to boost the efficiencies comparable with that of the devices with rigid substrates. The remaining challenge is to understand the vital role of the bulk heterojunction bends in extracting charge carriers and in achieving record efficiencies. Concerning the lead safety, assessing the impact of toxic lead to human beings and environmental is an ongoing hot topic as well.

Table 5 summarizes merits, weakness, and future development for several kinds of typical flexible active layers. As there is no toxic heavy metal used in fabrication processes and in final commercial finished products, a-Si:H cell is one of the most environmentally friendly photovoltaic devices. To overcome challenges in device efficiencies, successive efforts have been paid to push efficiencies towards the crystalline counterpart. Flexible organic solar cells have a huge potential due to its low-thermal budget fabrication using vapor phase deposition, spin-coating or roll-to-roll printing. Organic semiconductors are compatible with large-scaled flexible and stretchable substrates. With the removal of fullerene acceptors, organic active materials composed of conjugated polymers or small organics blending with non-fullerene acceptor have shown their merits in thermal stability, opening up an avenue for highly efficient and stable flexible organic solar cells. Furthermore, with the development of fused ring acceptors with electron deficit core (e.g., Y6)²⁰³, a series of organic active materials have enabled extending the light absorption threshold ~950 nm, which triggered considerable improvements in PCEs. The next few years promise to be exciting ones for research and development of high-efficiency flexible organic solar cells. For flexible perovskite solar cells, one of the key features is that they can

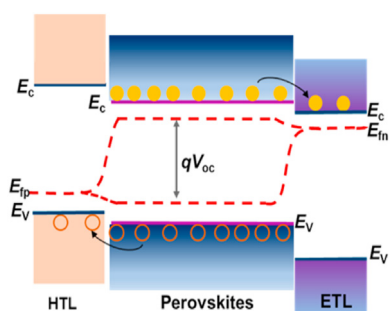


Fig. 11. A schematic of the working mechanism for perovskite solar cells. E_c and E_v represent the conduction band minimum and valence band maximum for semiconductors, respectively. E_{in} and E_{ip} are quasi-Fermi levels of electrons and holes, respectively.

Table 5

Summary of all sorts of perovskite active materials for best-performing solar cells. The a-Si:H is taken for reference.

Active materials	Merits	Weakness	Future development
a-Si:H ^{92,187,205,206}	<ul style="list-style-type: none"> - Reasonable carrier mobility $\sim 0.5\text{--}1.0\text{ cm}^2\text{ V}^{-1}\text{ s}^{-1}$; - Good mechanical flexibility; - Environmental stability. 	<ul style="list-style-type: none"> - Wide bandgap 1.77 eV; - Low device efficiencies; - Poor photostability. 	<ul style="list-style-type: none"> - a-Si:H/c-Si heterojunction cells.
MAPbI ₃ ^{189,207–211}	<ul style="list-style-type: none"> - High absorption coefficients; - Long carrier diffusion length; - Low temperature fabrication processes; - Abundant source materials such as PbI₂, PbCl₂, and Pb(Ac)₂, etc. 	<ul style="list-style-type: none"> - Wide bandgap 1.59 eV; - Poor environmental instability; - Ion migration; - A high density of defects; - Low power conversion efficiencies and stabilized power outputs. 	<ul style="list-style-type: none"> - Improve environmental instability; - Enhance device efficiencies for 1-sun-light illumination.
FAPbI ₃ ^{212,213}	<ul style="list-style-type: none"> - Narrow bandgap 1.51 eV; - Less ion migration; - Good heat stability; - Simple fabrication processes. 	<ul style="list-style-type: none"> - Phase instability of α-FAPbI₃ perovskites; - Low phase conversion temperature. 	<ul style="list-style-type: none"> - Stabilize α-FAPbI₃ phase; - Reduce defects.
CsPbI ₃ ^{214–216}	<ul style="list-style-type: none"> - Good thermal stability. 	<ul style="list-style-type: none"> - Phase instability, sensitive to the moisture; - Wide bandgaps 1.72 eV; - Low power conversion efficiencies. 	<ul style="list-style-type: none"> - Develop an effective means to stabilize the phase environmental stability; - Tandem perovskite-on-Si cell structures.
FA _{0.92} MA _{0.08} PbI ₃ ^{217,218}	<ul style="list-style-type: none"> - High light absorption coefficients $\sim 10^5$ and low voltage deficits; - Moderate defect densities; - Excellent phase stability; - Low Urbach energies; - High power conversion efficiencies. 	<ul style="list-style-type: none"> - Poor environmental stability; - Poor thermal stability under 1-sun-light illumination. 	<ul style="list-style-type: none"> - Replace a trace amount of MA⁺ with other cations; - Stabilize phase stability without compromising bandgaps.
FA _{0.83} Cs _{0.17} PbI _{2.4} Br _{0.6} ^{219,220}	<ul style="list-style-type: none"> - Resistant to the degradation after thermal stress <150 °C; - Excellent phase stability. 	<ul style="list-style-type: none"> - Low power conversion efficiencies; - Relatively wide bandgap 1.61 eV; - Low crystallization temperature. 	<ul style="list-style-type: none"> - Try other alkali ions constituting for Cs⁺; - Incorporate organic dopants; - Improve efficiencies.
FA _{0.81} MA _{0.14} Cs _{0.05} PbI _{2.55} Br _{0.45} ^{221–224}	<ul style="list-style-type: none"> - Superior thermal stability; - Low Urbach energies and voltage deficits; - High power conversion efficiencies and stabilized power output; - Improved reproducibility for batch-to-batch samples. 	<ul style="list-style-type: none"> - Relatively wide bandgaps 1.62 eV; - I/Br segregation and ion migration. 	<ul style="list-style-type: none"> - Mitigate the halogen redistribution induced by light illumination; - Further improve device performances on flexible substrates; - Optimize material chemical compositions.
FA _{0.77} MA _{0.14} Cs _{0.05} Rb _{0.03} PbI _{2.55} Br _{0.45} ^{225,226}	<ul style="list-style-type: none"> - Good thermal stability at an elevated temperature $\sim 85^\circ\text{C}$; - High open-circuit voltages; - Homogenize halide distribution over the film; - Improved long-term stability and operational stability at the maximum power point. 	<ul style="list-style-type: none"> - Relatively wide bandgaps $\sim 1.63\text{ eV}$; - Phase separation issues; - Complex compositions. 	<ul style="list-style-type: none"> - Clarify the vital role of Rb⁺ in multi-cation perovskites; - Scale up to large-area flexible devices; - Reduce the amount of Pb²⁺.
FA _{0.7} MA _{0.3} Pb _{0.5} Sn _{0.5} I ₃ ^{227,228}	<ul style="list-style-type: none"> - Extended light absorption to 1000 nm; - Offering the promise for perovskite-on-perovskite tandem cells; - A decrease in the fraction of the toxic divalent Pb²⁺; - High mobility $\sim 80\text{ cm}^2\text{ V}^{-1}\text{ s}^{-1}$. 	<ul style="list-style-type: none"> - Environmental and photo instability; - Relatively low power conversion efficiency; - Require very tight control of fabrication atmosphere. 	<ul style="list-style-type: none"> - Enhance the efficiency and operational stability; - Develop methods to suppress variation of the Sn²⁺ to Sn⁴⁺; - Develop solution scalable fabrication protocols.

be processed simply by scalable solution methods. The diversity in fabrication methods can give rise to low processing costs and simple implement of attractive flexible products. Evidence also suggests that perovskite solar cells can deliver better operational stability in space where moisture is low,²⁰⁴ indicating probable applications in aircrafts and drones.

4. Electrode materials

For most cases in device fabrications, a first layer of transparent and conducting electrode (TCE) is deposited on a transparent substrate, followed by a second layer of active materials, and then a third layer of reflective electrode. Fig. 2 (structure on the right) shows a transparent substrate with a TCE allowing light entering the active layer. The device structure shown on the left of Fig. 2 requires the top electrode transparent and the bottom one reflective. For transparent or semitransparent solar cells, both the top and the bottom electrodes must be transparent.

4.1. Transparent conducting oxide (TCO)

Transparent conducting oxides (TCO) are the most common electrodes in flexible solar cells. So far, ITO (tin-doped indium oxide) has

been the staple electrode material for solar cell industry.^{140,229,230} Large industrial scale ITO coated glass can be manufactured by magnetron sputtering. The work function of ITO films is 4.3–4.7 eV, which is neither close to the LUMO level nor to the HOMO level of most molecules applied in organic solar cells, therefore, numerous works have been carried out to modify ITO surfaces using methods such as UV-ozone, oxygen plasma, and chemical treatments.^{231,232} The WF of ITO electrode has been significantly improved up to 4.7–5.0 eV after treatments.^{233,234} It is worth mentioning that Helander et al.²³⁵ established a novel method to dramatically increase the WF to above 6 eV by ITO surface chlorination. Various thin-films, such as solution dissolved poly(3,4-ethylene dioxathiophene):polystyrene sulfonic acid (PEDOT:PSS) (WF $\sim 5.1\text{ eV}$), have been employed as anode surface modifier.^{236,237} Transition metal oxide like MoO_x, NiO, and WO_x have served as buffer layers between anode and active layers.^{238–241} Electron-selective layers composed of ZnO and TiO_x at cathode provide efficient electron collection and injection.^{242–246}

Although ITO is the most popular electrode, there are still several shortcomings challenging long-term applications.^{247–249} Limited supply of global indium is one of the biggest concerns for sustainable use of ITO. Moreover, the manufacturing of TVs, smartphones, solid state lightings, and other products also consume ITO and hence compete with solar panel production for ITO supplies.^{250–252} New oxides, ZnO-based compounds

such as Al-doped ZnO (AZO) and Ga-doped ZnO (GZO) have been shown as ITO-replacement.^{253,254} Demanding fabrication methods such as magnetron co-sputtering,²⁵⁵ are required for high-quality films deposition.^{256,257}

4.2. Thin metal films

Thick (>100 nm) metal (Al, Ag, and Mg) layers with high conductivity have been widely used as reflecting electrodes. When the thickness is reduced to below 20 nm, metal films become semitransparent.²⁵⁸ Those ultra-thin metal films have presented possible substitute to ITO in optoelectronic devices in laboratories.^{259–263} Efforts have been made to improve the over-all performance of ultra-thin metal films in device application, such as improving their transparency and conductivity.²⁶⁴ O'Connor et al.²⁶² demonstrated a device with a 9 nm thick Ag layer as the transparent electrode, exhibiting a competitive performance to the ITO device with the same CuPc/C₆₀ active bilayer structure.

Based on the good conductivity of thin metal films, Fan et al.²⁶⁵ reported a dielectric/thin metal/dielectric (DMD) multilayer structures to achieve high transparency and conductivity simultaneously. Looking into structure of DMD electrodes, the intermediate thin metal layer takes the responsibility of electrical conductance in the entire structure, while the two dielectric layers provide the high transparency of the electrode due to the surface plasmonic effects between the two metal/dielectric interfaces and the optical interference. There are many options for the dielectric layer materials including metal oxides (MoO₃,²⁶⁶ ZnO,²⁶⁷ WO₃,²⁶⁸ etc.), metal sulfide (e.g. ZnS²⁶⁹), and organic materials.²⁷⁰ The carrier injection/collection polarity is generally determined by the inner dielectric layers in these DMD electrodes structures. Other base metals (e.g., Al and Cu) have also been applied in DMD electrodes.²⁷¹

Metal grids, consisting of narrow (~1 μm) metal lines, are usually utilized in inorganic solar cells (e.g., Si-based solar cells and CIGS photovoltaic cells) as the front contacts.²⁷² To improve photocarrier harvesting, a conductive buffer layer (e.g., PEDOT:PSS) is used in solar cells²⁷³ and patterning of metal grids on flexible substrates is challenging.^{274,275} In 2013, Chen et al. reported a design of a PEDOT/Ag grid hybrid electrode as a current collector,²⁷⁶ and further implemented it in a large-area (active area of 1.21 cm²) flexible solar cell with a PCE of ~5.85% in 2014.²⁷⁷

Metal mesh is another form of thin-film electrode made by networks of periodic metal lines. The relatively large grains in the metal lines may produce additional light scattering and thus enhance light absorption by the active layer of the cell.²⁷⁸ Highly transparent Ag, Au and Cu mesh electrodes can be made by roll-to-roll compatible nanoimprint lithography technique and the corresponding device performance is comparable to that with commercial ITO electrodes.²⁷⁹ One challenging problem is the roughness of metal mesh surface,²⁸⁰ and the most common countermeasure is to deposit a thin planar layer on the top to form a hybrid metal mesh electrode. Significantly improved device performance, for instance, a PCE of 12.07% with a V_{oc} of 0.826 V, has been acquired by applying a composite inorganic-organic Ag mesh electrode.²⁸¹

4.3. Metal nanowires

Nano-structures of metal, such as copper,^{282,283} gold,^{284,285} and nickel,²⁸⁶ are regarded as promising electrodes. Since metal nanowires (NWs) can be well dispersed in various solvent after proper surface treatment, many solution-based processing techniques, including spin coating,²⁸⁷ spray coating,²⁸⁸ drop casting,²⁸⁹ doctor blade coating,²⁹⁰ Mayer rod coating,²⁹¹ and brush painting²⁹² have been developed to achieve flat films of NWs networks. Among all the NWs, Ag NWs provide both excellent electrical property and mechanical flexibility.

In general, an organic buffer layer (for example PEDOT:PSS) is necessary to planarize the surface of metal NW networks so that they can serve as either anodes (collect/inject holes) or cathodes (collect/inject

electrons).^{293–295} Such buffer layer also helps to reduce the interconnection barrier between active layer and electrodes. The overall performance of solar cells with Ag NW electrodes has been improved steadily. The inverted solar cell architecture was fabricated, resulting in a PCE of 3.5%, much higher than the PCE (2.0%) of cell with ITO.²⁸⁷ The excellent mechanical properties and conductivity suggest the strong potential of Ag NWs networks working as flexible transparent electrodes. Nevertheless, several challenges remain to be solved. The typical length of Ag NWs lies in the range of 1–50 μm, which is not long enough to maintain the integrity in networks and films. Short Ag NWs naturally tend to break during the deposition process.

4.4. Nano carbons

Novel carbon materials such as carbon nanotubes (CNTs) and graphene have attracted numerous attentions from academic and industrial community over the last 20 years due to their unique electrical, mechanical, and optical properties.

Extensive discussion had been carried out on the possibility of CNTs to apply as electrode materials in flexible solar cells from the early 2000.^{296–298} Depending on the number of layers, CNTs can be classified into two main categories: single-wall nanotubes (SWNTs)²⁹⁹ and multi-wall nanotubes (MWNTs).³⁰⁰ Both types of CNTs have been applied in optoelectronics as transparent electrodes. SWNTs exhibit higher transparency and conductivity³⁰¹ than MWNTs because of the difference in their optical transmittance under the same current density. For this reason, SWNTs are favored in many electronic devices as electrodes, replacing brittle ITO transparent electrodes.

Graphene, a single graphene sheet exhibits high in-plane conductance. In most cases, organic polymers such as PEDOT: PSS, and metal oxides (MoO₃, TiO₂, and ZnO) are widely utilized to modify graphene interface.

Chemical vapor deposition (CVD) is a successful technique for synthesizing SWNTs and achieving graphene films, which is still the most widely adopted approach to fabricate large carbonate sheets, despite its relatively high-cost and high treatment temperature.^{302–304} This technology has made a great deal of exciting progress on SWNTs and graphene electrodes fabrication.^{305,306} Recently, scientists are developing more efficient fabrication methods with lower cost for carbonate electrodes. Chirality-controlled production^{307,308} and high yield SWNTs cloning^{309–311} are considered other ideal concepts for producing SWNTs. Another alternative low-cost method for graphene electrode fabrication is to reduce graphene oxide, which provides a great opportunity to fabricate graphene inks or films on a large scale.^{312–315} Unfortunately, most graphene films produced by the reduction method show structural defects and high sheet resistance on the order of a 1 kΩ sq⁻¹ range, which is a result of contact resistances between graphene flakes.^{312,316} For large-area commercial applications, decreasing the resistance of the graphene layers along with simplifying the graphene fabrication/transfer processes needs to be further studied.

4.5. Conducting polymers

PEDOT:PSS has been commonly introduced in organic optoelectronics as an interlayer since its discovery in the 1990s. The main role of PEDOT:PSS was to reduce the roughness of ITO surface and increase the hole collection/injection rate between the active layers and ITO electrode.³¹⁷ PEDOT:PSS polymers have been investigated as alternative low-cost electrodes by various groups^{318,319} because their outstanding superiorities in optical properties, processability, and compatibility with flexible applications. The biggest challenge of polymers as electrodes is improving their electrical conductivities. Hence, numerous attempts have been made to optimize the electrical conductivity of polymers by suitable chemical doping. These dopants include polyaniline, polypyrrole, and polythiophene.^{320–322}

Solvent with high boiling temperature contributes to enhancing the

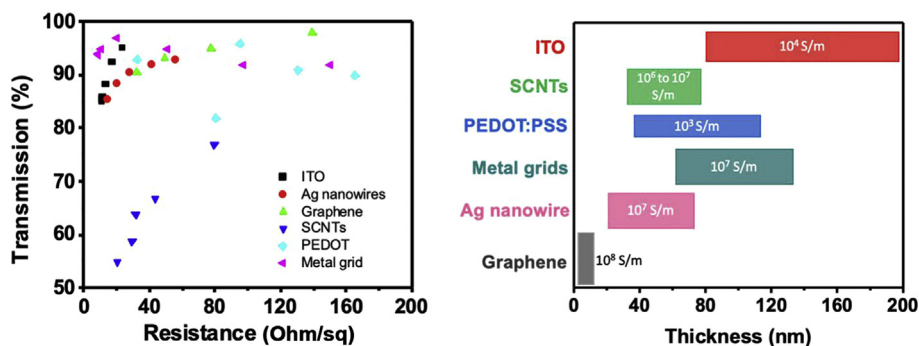


Fig. 12. The electrode sheet resistance vs optical transmission ($\lambda = 550$ nm) of several electrode materials (left). Typical range of thicknesses for various electrode materials used in solar cells (right).

conductivity of polymers. Reported data shows that polar molecules such as dimethylsulfoxide (DMSO),^{323,324} ethylene glycol (EG),^{325,326} diethylene glycol,³²⁷ and sorbitol³²⁸ can increase the conductivity of PEDOT:PSS by more than one order of magnitude. For example, Kim et al. reported that the conductivity of a PEDOT:PSS film with the addition of 6 vol% EG could achieve a conductivity of $\sim 1418 \text{ S cm}^{-1}$.³²² Formic acid has been reported to improve PEDOT:PSS conductivity to 2050 S cm^{-1} .³²⁹ These recent reports show that PEDOT:PSS has the potential to gain comparable conductivity with ITO's, and is expected to be used for top transparent electrodes. The polymer electrodes also have the inherent advantage of low-temperature processing such as spin-coating, spray, ink-printing, and stamp-transfer lamination.³³⁰

4.6. Properties summary

Mechanical property: Mechanical property is a key consideration in selecting electrodes for flexible solar cells. TCO is essentially a ceramic material resistant to elastic deformation. In 2017, Hengst et al.³³¹ investigated the elastic behavior of ITO and ZTO films as electrodes in flexible a-Si:H solar cells. The Young's moduli of both TCO films were around 100 GPa at 1 μm and found to decrease with increasing thickness. The tensile test also showed that ITO films have a total elongation and yield strength of 0.003 and 300 MPa, respectively. This is a problem for application in flexible solar cells. However, numerous companies and research groups are working on methods to engineer the TCO film's flexibility. For example, Kim et al.³³² developed a flexible TCO middle electrodes for tandem OPV by inserting an alkali metal carbonate interfacial layer. Because of their technology maturity, TCO electrodes are conveniently used for a-Si:H,^{333,334} organic molecule,³³² and perovskite cells.^{335,336}

Polymers have the smallest Young's moduli of 1–3 GPa at 1 μm , therefore, bending and stretching polymer electrodes are much easier than TCO electrodes. Additionally, the total elongation of polymer (0.02–0.06), while with a relatively low yield strength (10–50 MPa), is more than 10 times greater than that of TCOs.³³⁷

The mechanical flexibility and durability of metal-composite electrodes are between that of polymers and TCO. Most literatures use bending tests to evaluate the mechanical robustness of electrode materials. Two parameters are commonly cited: (1) bending radius and (2) bending cycles. Cao et al.³³⁸ successfully designed a flexible P3HT:PCBM device with $\text{MoO}_x/\text{Au}/\text{MoO}_x$ electrode on PET substrates, and further studied the fatigue strength of the device using bending test. Only a $\sim 6\%$ drop in efficiency was observed after 500 bending cycles at a bending radius of 1.3 cm. Metal NWs networks show great advantages on mechanical properties as the thin metal films.^{291,339–341} Ag NWs can be used as top electrode of both organic²⁹¹ and inorganic perovskite solar cells.³⁴² Hybrid Ag grid/PEDOT:PSS electrode has been found highly flexible with a durability of up to 10000 bending cycles.³⁴³

Nano carbon electrodes also showed compatible flexibility as metal-

composite electrodes. In the flexible solid-state perovskite solar cell developed by Wong et al.,¹⁵ a transparent SWNTs top electrode shows little performance deterioration after 100 mechanical bending cycles. SWNTs can also be doped by other particles to enhance overall performance. Lee et al.³⁴⁴ combined TiO_2 and metallic SWNTs together as a photo anode for flexible DSSCs fabrication. A robust device based on a Ti foil using metallic SWNTs/ TiO_2 electrode was demonstrated to have good flexibility and stability in PCE after 1000 bending cycles.

Optical transparency: Doped metal oxide thin films exhibit high transparency ($>80\%$ absorption transmittance) due to the wide bandgap of most metal oxides. For ITO and ZnO they both have a wide bandgap (>3 eV) and are almost transparent (80–95%) in the visible spectral range. Transparency is a weakness of metallic materials. For the thin metal films, the transparency changes dramatically with thicknesses. A maximum transmittance of $\sim 70\%$ at $\lambda = 500$ nm was obtained for a 7-nm-thick Au film, which was reduced to $<60\%$ for a 12-nm-thick film. Metal NWs films are comparable with standard ITO electrodes with transmittance $>85\%$ as well, and sheet resistance $<20 \Omega \text{ sq}^{-1}$. Many groups have explored them as transparent electrodes in organic optoelectronic devices.^{248,287,345} High-quality films require delicately controlling of the metal NWs diameter, compact films provide the conductive pathways for charge carrier transport, but they also function as scatter centers to incident light affecting the optical properties of the films. Therefore, the diameter of metal NWs should be large enough to maximize current flow and small enough to achieve high optical transparency.

Nano carbons can also achieve high transmittance. Graphene is the most promising materials for transparent electrodes because of its excellent optical properties: a single graphene layer has a theoretical transmittance of 97.7% (with a reflectance of 0.1% and absorbance of $\sim 2.3\%$).^{346,347} Maruyama et al.³⁴⁸ demonstrated a flexible organic solar cell with metallic SWNT-based transparent front electrode.

Electrical conductivity: Electrical conductivity is another key parameter. There exists a trade-off between sheet resistance and optical transparency features mentioned above. Assuming the electrode material is homogeneous without any surface or interface effects, we specify σ , α , t are the electrical conductivity, absorption coefficient, and thickness of the electrode, respectively, then, the sheet resistance of the electrode, R_{sh} , should be inversely proportional to the thickness $R_{sh} = \frac{1}{\sigma t}$, whereas the transparency, T , follows an exponential decay behavior with t as $T = e^{-\alpha t}$ according to the Lambert-Beer law. Hence increasing the electrode thickness leads to lowering in both sheet resistance and transparency (see Fig. 12).

Doped metal ions create extrinsic charge carrier and increase the conductivity of oxide films.^{349,350} Commercial ITO thin films with thickness between 100 and 300 nm usually have good sheet resistances of $\sim 20 \Omega \text{ sq}^{-1}$, corresponding to the conductivities of $\sim 10^3 \text{ S cm}^{-1}$. Dopants like Al and Ga, are added into the ZnO films to improve the conductivity by introducing ionic impurities to the films, but the sheet resistance is slightly higher ($\sim 50 \Omega \text{ sq}^{-1}$) than ITO.

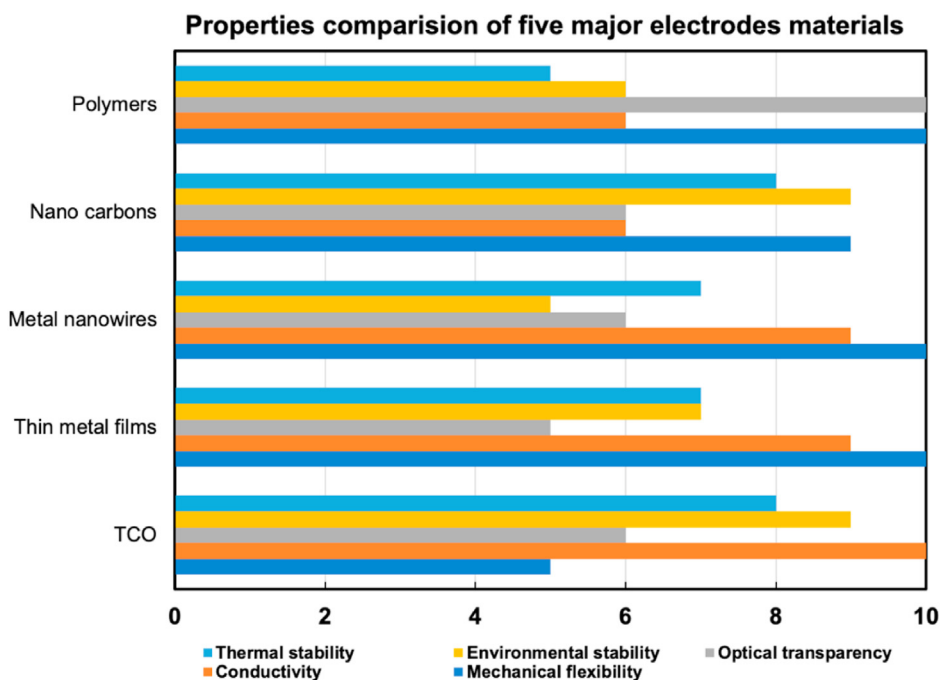


Fig. 13. Comparison of relative physical properties of various electrode materials. The numerical number of the bar length indicates poor (5) to excellent (10) in meeting the requirement for a flexible transparent electrode.

Conductivity is a great advantage of thin metal materials. Wilken et al.²⁶³ measured the sheet resistance of Au thin films with different thicknesses (10–60 nm). They found that the experimental sheet resistance qualitatively followed the predicted trend of the Fuchs-Sondheimer and Mayadas-Shatzkes models, showing the relationship between thickness and sheet resistance. The Au film has a low sheet resistance of $<5 \Omega \text{ sq}^{-1}$ when the thicknesses $>20 \text{ nm}$, while it dramatically increases to $>50 \Omega \text{ sq}^{-1}$ for films $<10 \text{ nm}$.

Metal NWs are almost as good as thin metal films in terms of conductivity. Some groups have reported Ag NWs materials with sheet resistance $<20 \Omega \text{ sq}^{-1}$, and explored them as transparent electrodes in organic optoelectronic devices.^{248,287,345} It should be pointed out that the junction resistance between the jointed wires is another dominant factor that affects the film resistance. There are several modification methods to reduce the junction resistance such as optical sintering,³⁵¹ mechanical pressing,³⁵² thermal annealing,^{353,354} fusing with other materials,³⁵⁵ and effectively improve the film conductivity.

For nano carbons, conductivity varies from a single molecule to organized films. Individual SWNTs have charge mobilities of $10^5 \text{ cm}^2 \text{ V}^{-1} \text{ s}^{-1}$ and electrical conductivities in the range of $1\text{--}3 \times 10^6 \text{ S m}^{-1}$.^{247,356} Though individual nanotubes showed excellent electrical properties, films comprised by a network of CNTs present extremely low conductivity and mobility as a result of the magnitude contact resistance between CNTs.²⁴⁷ Besides, the poor interconnection between CNTs combined with rough surfaces of CNT films lead to a high sheet resistance ($>200 \Omega \text{ sq}^{-1}$), restraining their applications in optoelectronic devices. Graphene faces the same situation with CNTs, single graphene sheet exhibits a low sheet resistance of $<100 \Omega \text{ sq}^{-1}$, however, the number boosts to the order of $1 \text{ k}\Omega \text{ sq}^{-1}$ for graphene films. Poor conductivity is the biggest obstacle for nano carbons as electrodes.

Environmental Stability: The device service lifetime is dependent on the environmental stability of materials. Electrodes need to work properly over a wide temperature range and be stable against exposure to moisture, oxygen and sun radiation. The degradation in conductivity upon environment exposure will lead to device breakdown.^{357,358}

The CNTs are composed entirely of sp^2 chemical bonds, which are very strong and accordingly provide CNTs with outstanding strength. The

CNTs is estimated to be thermally stable at temperature of up to 2800°C in vacuum or around 750°C in air.³⁵⁹ However, it is quite different in the case of CNTs as electrodes in devices. Doping is usually essential for further performance improvement, common doping substances include inorganic solvents³⁶⁰ (HNO_3 and SOCl_2), MoO_3 ,³⁶¹ and copper halides,³⁶² etc. The conductivity of CNTs films can be greatly enhanced through chemically doping treatment, further resulting in the enhancement of charge carrier and decrease of contact resistance of CNT-CNT junction. Obviously, doped CNT films become sensitive to air, temperature, or humidity. Thus, most of the reported CNTs electrodes are not stable.

Thermal stability: Metal oxide films are superior in thermal stability. Nevertheless, high temperature fabricating process may damage the underlying semiconductors.^{363,364} It is necessary to apply some buffer layers or sacrificial layers, such as organic/inorganic protective layers^{365,366} (copper phthalocyanine, Mg/Ag layer, etc) to protect the underlying active layer when using ITO as the top electrode. Successful cases have been reported in fabricating electrodes with low-energy magnetron sputtering method,^{367–369} however, the optical and electronic properties for these ITO layers are still far away from commercialization.³⁶⁶

The thermal stability of NWs can be improved by enlarging their diameters: the thinner they are, the lower the temperature associated with the NWs' thermal instability.³⁷⁰ However, it seems that using hybrid materials combining NWs and thin layers of other materials is a much more promising way of drastically restraining the effects of such instability. For instance, introducing reduced graphene oxide in either Ag NWs³⁷¹ or Cu NWs³⁷² has been shown to be beneficial to the robustness and stability of the resulting films. Embedding Ag NWs with either ZnO nanoparticles²⁹⁴ or a TiO_2 layer³⁷³ was found to be an effective way to significantly improve the thermal stability. More specifically, utilization of atomic layer deposition (ALD) makes possible the deposition of very conformal and homogeneous thin protecting layers (just a few nm) without significantly impacting the transparency of the films, while improving the contact between the NWs network and the underlying substrate at the same time.³⁷⁴

Ab initio calculations show that nano carbons are thermodynamically

Table 6

Summary table of different electrode materials commonly used in flexible solar cells.

Metal oxide materials	Merits	Weakness	Future development
ITO ^{140,229,230}	<ul style="list-style-type: none"> - Good thermal stability; - High optically transparency (>90%); - Low sheet resistance (<20 Ω sq⁻¹); - Mature manufacturing. 	<ul style="list-style-type: none"> - Poor mechanical flexibility; - High deposition temperature (>300 °C); - High cost of indium (~\$110/lb). 	<ul style="list-style-type: none"> - Recycle of indium from waste.
Doped ZnO ^{242–246}	<ul style="list-style-type: none"> - High optically transparency (80%–95%); - High thermal stability; - Low material cost (~\$20/lb). 	<ul style="list-style-type: none"> - Relatively high sheet resistance (~50 Ω sq⁻¹); 	<ul style="list-style-type: none"> - Improve sheet resistance.
Thin metal films ^{259–263}	<ul style="list-style-type: none"> - Low sheet resistance (1–80 Ω sq⁻¹); - Excellent mechanical flexibility; - Low thermal budget deposition. 	<ul style="list-style-type: none"> - Poor transparency (40–60%); 	<ul style="list-style-type: none"> - Develop combined metal films grid fabrication to improve optical transparency.
Metal grid ^{274,275}	<ul style="list-style-type: none"> - High transparency (~80%); - Low sheet resistance (6–50 Ω sq⁻¹); - Excellent mechanical flexibility. 	<ul style="list-style-type: none"> - Reduced photocarrier harvesting area. 	<ul style="list-style-type: none"> - Develop combined metal films and metal grid to improve harvesting of charge carrier.
Ag NWs ^{293–295}	<ul style="list-style-type: none"> - Excellent mechanical flexibility; - Stretchable; - Relative high conductivity (sheet resistance < 20 Ω sq⁻¹); - Good optical transmittance (>85%). 	<ul style="list-style-type: none"> - Low environmental stability; - Sensitive to humidity and oxygen. 	<ul style="list-style-type: none"> - Reduce cost.
SWNTs ^{299,301}	<ul style="list-style-type: none"> - Ability to conform to non-planar surface. - Excellent mechanical strength; - High thermal conductivity and stability; - Good transparency (50%–90%); - Good conductivity (20–1000 Ω sq⁻¹). - Solution processability. 	<ul style="list-style-type: none"> - Insufficient electronic conductivity; - Low surface contact area. 	<ul style="list-style-type: none"> - improve film surface morphology.
Graphene ^{312–315}	<ul style="list-style-type: none"> - Excellent conductivity; - Fast charge carrier mobility (550 S cm⁻¹ in a ~10 nm film); - Good mechanical strength; - high optical transparency (>95%). 	<ul style="list-style-type: none"> - High cost fabrication; - Poor film formation; - Poor film stability. 	<ul style="list-style-type: none"> - Develop better method for making films; - Enhance solubility in organic solvent;
PEDOT:PSS ^{318,319}	<ul style="list-style-type: none"> - Good optical properties (transparency up to 95%); - Good mechanical flexibility; - Good interfacial contact with organic materials. 	<ul style="list-style-type: none"> - Degrade easily under humidity and UV exposure; - Poor thermal stability; - Poor operational stability. 	<ul style="list-style-type: none"> - Improve electrical properties; - Improve environmental stability.

stable if their sizes are larger than 20 nm. Many cases have proved the thermal stability of CNTs and graphene in air. It is found that single-layer graphene starts to show defects at ~500 °C, while this happens at ~600 °C for bilayer graphene, indicated by the appearance of a disorder-induced Raman D peak.³⁷⁵ Additionally, single-layer graphene is repeatedly reported with a thermal-conductivity of ~5000 W mK⁻¹ at 25 °C, which is the result of the presence of phonon scattering property and strong C–C covalent bonds.

Fig. 13 presents a comparison of five key material properties for different electrode materials used for flexible solar cells. The bar length indicates relative performance. The selection of electrode material for a particular type of flexible solar cells requires comprehensive consideration of the process flow and temperature budget in fabrication.

4.7. Future development in electrode materials

Last but not the least, interfaces at substrate/electrode/active materials are crucial factors when evaluating a candidate material for the electrodes. It is a challenge to apply suitable electrode materials that can form good interface contact without impacting active layers. Table 6 provides several examples of metal oxide, thin metal films, metal-organic composite, carbon materials and gives a detailed comparison between materials of each category.

In the near future, ITOs will continue to play a significant role in commercial production of silicon and CIGS based flexible solar cells. To reduce the cost of metal oxides, more and more indium-free materials, such as AZO and GZO, are investigated and utilized as transparent electrodes. Another type of metal oxide electrode, fluorine-doped tin-oxide (FTO), is also widely employed as electron collection electrodes in DSSCs.^{376,377} Most recently, FTOs have also been broadly used as bottom transparent cathodes in inverted planar heterojunction solar cells due to the rapid development of new photovoltaic active materials,

perovskite.^{378,379}

Thin metals films are also promising transparent electrodes. A few studies aimed to increase the optical transparency without sacrificing the electrical conductivity,^{380–382} such as applying a seed layer to improve the morphology of thin metal layers.³⁸³ To further reduce the cost of achieving uniformity of ultrathin DMD and metal grid layers, better deposition methods are investigated such as nanoimprint lithography (NIL) technique.³⁸⁴

In the far future, nano carbons may emerge as attractive alternative to ITO. However, great efforts should be made on approaching commercial applications because of their low film conductivities and between-layer contact. Many film treatment methods were developed for achieving CNTs electrodes with higher electrical conductivity and smoother film surface.^{385–388}

A new trend of electrode research is to make hybrid materials. The combination of two or more materials, such as metal grid/polymer, metal NWs/polymer, graphene/metal grids, thin metal/graphene, etc., brings about improved performance as transparent electrodes by complementing the good properties of each material.^{389,390} This also opens up more routes for developing new electrodes for flexible solar cells.

5. Conclusion and perspective

This paper provides a comprehensive review of key materials (including substrates, electrodes, and active materials) for fabricating flexible solar cells. Substrate materials reviewed here include metals, ceramics, glass, and plastics. Despite advances in flexible substrates, a new and/or improved substrate is still needed to satisfy the requirement of flexibility and low-cost products. Stainless steel is expected to be the dominate material in near future. For plastic PI substrates, it is crucial to develop cost-effective method to apply moisture barrier coating. For

flexible ceramic/glass substrate, the challenge is to fabricate large-scale substrate cheaply. For the active materials, we reviewed a-Si:H, CIGS, small molecular organic semiconductors, conjugated polymer semiconductors, and organometal halide perovskites. a-Si:H and CIGS are expected to dominate the market in near future. However, owing to their high efficiency and low-temperature fabrication, commercial development of perovskite and non-fullerene organic solar cells are expected to accelerate. For electrode materials, transparent conducting oxides will continue to dominate. Research to discover new materials such as conducting nano-composite materials and conducting polymers is expected to intensify.

Declaration of competing interest

There is no conflict to declare.

Acknowledgements

Z.H. Lu would like to acknowledge the Natural Science and Engineering Research Council of Canada, and the National Natural Science Foundation of China (Grant No. 11774304) for providing research fund. H.Y. Yu would like to acknowledge the financial support by Research and Application of Key Technologies of GaN-based Power Devices on Si Substrate (Grant No: 2019B010128001), Research on key technologies for optimization of IoT chips and product development (Grant No. 2019B010142001), and Study and optimization of electrostatic discharge mechanism for GaN HEMT devices (Grant No: JCYJ20180305180619573) and Research of AlGaIn HEMT MEMS sensor for work in extreme environment (Grant No: JCYJ20170412153356899). The authors thank Toyota Motor Corporation for its product photo supply.

References

- Shirland F, Wolff G. *Research on Solar-Energy Conversion Employing Cadmium Sulfide*. 2. Cleveland OH: Harshaw Chemical Co; 1962.
- Vohl P, Perkins D, Ellis S, Addiss R, Hui W, Noel G. GaAs thin-film solar cells. *IEEE Trans Electron Dev*. 1967;14:26–30.
- Williams E, Jones K, Griffiths A, et al. The electrophoresis of thin Film CdS/Cu₂S solar cells. *Sol Cell*. 1980;1:357–366.
- Okaniwa H, Nakatani K, Yano M, Asano M, Suzuki K. Preparation and properties of a-Si: H solar cells on organic polymer film substrate. *Jpn J Appl Phys*. 1982;21:239.
- Dursch H. *CDS/CUINSE/sub 2/solar Cells with Titanium Foil Substrate*. 1987.
- Yano M, Suzuki K, Nakatani K, Okaniwa H. Roll-to-roll preparation of a hydrogenated amorphous silicon solar cell on a polymer film substrate. *Thin Solid Films*. 1987;146:75–81.
- Fonrodona M, Escarré J, Villar F, et al. PEN as substrate for new solar cell technologies. *Sol Energy Mater Sol Cells*. 2005;89:37–47.
- Ishizuka S, Yamada A, Matsubara K, Fons P, Sakurai K, Niki S. Alkali incorporation control in Cu (In, Ga) Se₂ thin films using silicate thin layers and applications in enhancing flexible solar cell efficiency. *Appl Phys Lett*. 2008;93:124105.
- Ding JM, de la Fuente Vornbrock A, Ting C, Subramanian V. Patternable polymer bulk heterojunction photovoltaic cells on plastic by rotogravure printing. *Sol Energy Mater Sol Cells*. 2009;93:459–464.
- Rance W, Burst J, Reese M, et al. In The use of Corning® Willow™ glass for flexible CdTe solar cells. In: *2013 IEEE 39th Photovoltaic Specialists Conference (PVSC)*. IEEE; 2013:1649–1652.
- Wong WS, Salleo A. *Flexible Electronics: Materials and Applications*. 11. Springer Science & Business Media; 2009.
- Carlson DE. Amorphous-silicon solar cells. *IEEE Trans Electron Dev*. 1989;36:2775–2780.
- Xiao Y, Han G, Zhou H, Wu J. An efficient titanium foil based perovskite solar cell: using a titanium dioxide nanowire array anode and transparent poly (3, 4-ethylene-dioxythiophene) electrode. *RSC Adv*. 2016;6:2778–2784.
- Kim M, Yun H-G, Jang L-W, et al. Promising efficiency enhancement in cobalt redox couple-based back-illuminated dye-sensitized solar cells with titanium foil substrate. *J Power Sources*. 2015;278:32–37.
- Wang X, Li Z, Xu W, et al. TiO₂ nanotube arrays based flexible perovskite solar cells with transparent carbon nanotube electrode. *Nano Energy*. 2015;11:728–735.
- Sheehan S, Suroli P, Byrne O, et al. Flexible glass substrate based dye sensitized solar cells. *Sol Energy Mater Sol Cells*. 2015;132:237–244.
- Dou B, Miller EM, Christians JA, et al. High-performance flexible perovskite solar cells on ultrathin glass: implications of the TCO. *The journal of physical chemistry letters*. 2017;8:4960–4966.
- Formica N, Mantilla-Perez P, Ghosh DS, et al. An indium tin oxide-free polymer solar cell on flexible glass. *ACS Appl Mater Interfaces*. 2015;7:4541–4548.
- Ishizuka S, Yamada A, Matsubara K, Fons P, Sakurai K, Niki S. Development of high-efficiency flexible Cu (In, Ga) Se₂ solar cells: a study of alkali doping effects on CIS, CIGS, and CGS using alkali-silicate glass thin layers. *Curr Appl Phys*. 2010;10:S154–S156.
- Todorov T, Olenick J, Aolenick K, et al. In Flexible kesterite solar cells on ceramic substrates for advanced thermal processing. In: *2015 IEEE 42nd Photovoltaic Specialist Conference (PVSC)*. IEEE; 2015:1–3.
- Yoon H, Kang SM, Lee J-K, Choi M. Hysteresis-free low-temperature-processed planar perovskite solar cells with 19.1% efficiency. *Energy Environ Sci*. 2016;9:2262–2266.
- Hanada T, Negishi T, Shiroishi I, Shiro T. Plastic substrate with gas barrier layer and transparent conductive oxide thin film for flexible displays. *Thin Solid Films*. 2010;518:3089–3092.
- Burrows PE, Graff GL, Gross ME, et al. Ultra barrier flexible substrates for flat panel displays. *Displays*. 2001;22:65–69.
- Henry B, Erlat A, McGuigan A, et al. Characterization of transparent aluminium oxide and indium tin oxide layers on polymer substrates. *Thin Solid Films*. 2001;382:194–201.
- Koch C, Ito M, Schubert M. Low-temperature deposition of amorphous silicon solar cells. *Sol Energy Mater Sol Cells*. 2001;68:227–236.
- Ong KH, Agileswari R, Maniscalco B, et al. Review on substrate and molybdenum back contact in CIGS thin film solar cell. *Int J Photoenergy*. 2018;9106269, 2018.
- Kaltenbrunner M, White MS, Glowacki ED, et al. Ultrathin and lightweight organic solar cells with high flexibility. *Nat Commun*. 2012;3:770.
- Kapur VK, Bansal A, Le P, Asensio OL. Non-vacuum processing of CuIn_{1-x}Ga_xSe₂ solar cells on rigid and flexible substrates using nanoparticle precursor inks. *Thin Solid Films*. 2003;431:53–57.
- Van Den Berg G. The effect of the non-linear stress-strain behaviour of stainless steels on member capacity. *J Constr Steel Res*. 2000;54:135–160.
- Kese K, Li Z, Bergman B. Influence of residual stress on elastic modulus and hardness of soda-lime glass measured by nanoindentation. *J Mater Res*. 2004;19:3109–3119.
- Amborski LE, Flierl DW. Physical properties of polyethylene terephthalate films. *Ind Eng Chem*. 1953;45:2290–2295.
- Callister WD, Rethwisch DG. *Materials Science and Engineering: An Introduction*. 7. John Wiley & sons New York; 2007.
- Awaja F, Pavel D. Recycling of PET. *Eur Polym J*. 2005;41:1453–1477.
- Aref-Azar A, Biddlestone F, Hay J, Haward R. The effect of physical ageing on the properties of poly (ethylene terephthalate). *Polymer*. 1983;24:1245–1251.
- Alizadeh-Sh M, Marashi S, Pouranvari M. Resistance spot welding of AISI 430 ferritic stainless steel: phase transformations and mechanical properties. *Mater Des*. 2014;56:258–263, 1980–2015.
- Fogaing EY, Lorgouilloux Y, Huger M, Gault C. Young's modulus of zirconia at high temperature. *J Mater Sci*. 2006;41:7663–7666.
- Cros S, De Bettignies R, Berson S, et al. Definition of encapsulation barrier requirements: a method applied to organic solar cells. *Sol Energy Mater Sol Cells*. 2011;95:S65–S69.
- Choy WC. *Organic Solar Cells: Materials and Device Physics*. Springer; 2012.
- Hwa Hong K, Jin Kang T. Hydraulic permeabilities of PET and nylon 6 electrospun fiber webs. *J Appl Polym Sci*. 2006;100:167–177.
- Ito H, Oka W, Goto H, Umeda H. Plastic substrates for flexible displays. *Jpn J Appl Phys*. 2006;45:4325.
- Lewis JS, Weaver MS. Thin-film permeation-barrier technology for flexible organic light-emitting devices. *IEEE J Sel Top Quant Electron*. 2004;10:45–57.
- Fahlteich J, Fahlend M, Schönberger W, Schiller N. Permeation barrier properties of thin oxide films on flexible polymer substrates. *Thin Solid Films*. 2009;517:3075–3080.
- Crawford GP. *Flexible Flat Panel Display Technology*. Wiley Online Library 2005 Vol. 3.
- Huang J-M, Chu P, Chang F-C. Conformational changes and molecular motion of poly (ethylene terephthalate) annealed above glass transition temperature. *Polymer*. 2000;41:1741–1748.
- Fan CF, Çagin T, Shi W, Smith KA. Local chain dynamics of a model polycarbonate near glass transition temperature: a molecular dynamics simulation. *Macromol Theory Simul*. 1997;6:83–102.
- Yokota R, Yamamoto S, Yano S, et al. Molecular design of heat resistant polyimides having excellent processability and high glass transition temperature. *High Perform Polym*. 2001;13:S61–S72.
- Ravindranath K, Malhotra S. The influence of aging on the intergranular corrosion of 22 chromium-5 nickel duplex stainless steel. *Corrosion Sci*. 1995;37:121–132.
- Pan J, Thierry D, Leygraf C. Electrochemical impedance spectroscopy study of the passive oxide film on titanium for implant application. *Electrochim Acta*. 1996;41:1143–1153.
- Kolli M, Hamidouche M, Bouaouadja N, Fantozzi G. HF etching effect on sandblasted soda-lime glass properties. *J Eur Ceram Soc*. 2009;29:2697–2704.
- Venkatachalam S, Nayak SG, Labde JV, Gharal PR, Rao K, Kelkar AK. Degradation and recyclability of poly (ethylene terephthalate). In: *Polyester*. InTech India; 2012: 75–98.
- Nagai N, Matsunobe T, Imai T. Infrared analysis of depth profiles in UV-photochemical degradation of polymers. *Polym Degrad Stabil*. 2005;88:224–233.
- Karlsson T, Roos A. Optical properties and spectral selectivity of copper oxide on stainless steel. *Sol Energy Mater*. 1984;10:105–119.
- Lee C, Park A, Cho Y, Park M, Lee WI, Kim HW. Influence of ZnO buffer layer thickness on the electrical and optical properties of indium zinc oxide thin films deposited on PET substrates. *Ceram Int*. 2008;34:1093–1096.

54. Ni H-j, Liu J-g, Wang Z-h, Yang S-y. A review on colorless and optically transparent polyimide films: chemistry, process and engineering applications. *J Ind Eng Chem.* 2015;28:16–27.
55. MetalMiner. *Stainless Steel*; 2019. <https://agmetalmminer.com/metal-prices/stainless-steel>.
56. Steel Cooperation AK. *304/304L Stainless Steel*; 2019. <https://www.aksteel.com/sites/default/files/2018-11/304-304l-stainless.pdf>.
57. Afentakis T, Hatalis M, Voutsas AT, Hartzell J. Design and fabrication of high-performance polycrystalline silicon thin-film transistor circuits on flexible steel foils. *IEEE Trans Electron Dev.* 2006;53:815–822.
58. Steel Cooperation AK. *430 Stainless Steel*; 2019. <https://www.aksteel.com/sites/default/files/2018-11/430-stainless.pdf>.
59. Wu C, Theiuss S, Gu G, et al. Integration of organic LEDs and amorphous Si TFTs onto flexible and lightweight metal foil substrates. *IEEE Electron Device Lett.* 1997; 18:609–612.
60. MetalMiner Aluminum. <https://agmetalmminer.com/metal-prices/aluminum>; 2019.
61. Metals Comet. *Aluminum Alloy Guide*; 2019. https://cometmetals.com/wp-content/uploads/2018/10/Aluminum_Alloy_guide.pdf.
62. Shingu A, Ooyagi M. *Aluminum foil, electronic device, roll-to-roll aluminum foil, and method of producing aluminum foil*. Google Patents; 2019.
63. Handbook A. *Properties of wrought aluminum and aluminum alloys*. In: *ASM International Hand Book Committee*. 2. 1990:62–122.
64. Kaufman JG. *Fire Resistance of Aluminum and Aluminum Alloys*. 2016.
65. Kanjer, A.; Optasanu, V.; Lavis, L., et al, High Temperature Oxidation Behaviour of Titanium after Shot-Peening..
66. Rmititanium Co L. *Titanium Alloy Guide*. 2000.
67. Kulkarni M, Patil-Sen Y, Junkar I, Kulkarni CV, Lorenzetti M, Igljć A. Wettability studies of topologically distinct titanium surfaces. *Colloids Surf B Biointerfaces.* 2015; 129:47–53.
68. Focus Technology Co L. *0.2mm Clear Ultra-thin Soda-Lime Glass for Optical Glass*. 2019.
69. Ashby MF. *Materials and the Environment: Eco-Informed Material Choice*. Elsevier; 2012.
70. International Syalons. (Newcastle) Limited, *Zirconia*; 2019. <https://www.syalons.com/materials/zirconia/>.
71. Ceramics SST. *Zirconia Ceramic Materials*. 2019.
72. Inframcat Advanced Materials. *Zirconia Powder*; 2019. <http://www.advancedmaterials.us/40R-0801.htm>.
73. Insight Plastic. *Polyethylene Terephthalate (PET): Production, Price, Market and its Properties*; 2019. <https://www.plasticsinsight.com/resin-intelligence/resin-prices/polyethylene-terephthalate>.
74. Orlando G. *Regenerative Medicine Applications in Organ Transplantation*. Academic Press; 2013.
75. Singh N, Qureshi A, Shah N, et al. Surface modification of polyethylene terephthalate by plasma treatment. *Radiat Meas.* 2005;40:746–749.
76. Anand K A, Agarwal U, Joseph R. Carbon nanotubes-reinforced PET nanocomposite by melt-compounding. *J Appl Polym Sci.* 2007;104:3090–3095.
77. Materials A. *Polyethylene Naphthalate (PEN) - Data Supplied by Goodfellow*. 2003.
78. Arkhireyeva A, Hashemi S. Fracture behaviour of polyethylene naphthalate (PEN). *Polymer.* 2002;43:289–300.
79. Alibabacom. *Polyethylene Naphthalate (PEN)*; 2019. <https://www.alibaba.com/product-detail/Polyethylene-Naphthalate-PEN-50030309775.html?spm=a2700.7724857.normalList.2.6ea5278f0aePn3>.
80. *Plastic Insight, Polycarbonate Properties, Production, Price, Market and Uses*; 2019. <https://www.plasticsinsight.com/resin-intelligence/resin-prices/polycarbonate/>.
81. Adam G, Cross A, Haward R. The effect of thermal pretreatment on the mechanical properties of polycarbonate. *J Mater Sci.* 1975;10:1582–1590.
82. Barlow C, Kumar V, Flinn B, Bordia RK, Weller J. Impact strength of high density solid-state microcellular polycarbonate foams. *J Eng Mater Technol.* 2000;123: 229–233.
83. Xie L, Gidley DW, Hristov HA, Yee AF. Evolution of nanometer voids in polycarbonate under mechanical stress and thermal expansion using positron spectroscopy. *J Polym Sci, Part B: Polym Phys.* 1995;33:77–84.
84. Sekkat Z, Wood J, Knoll W, Volksen W, Miller RD, Knoesen A. Light-induced orientation in azo-polyimide polymers 325° C below the glass transition temperature. *JOSA B.* 1997;14:829–833.
85. Küper S, Brannon J. Ambient gas effects on debris formed during KrF laser ablation of polyimide. In: *MRS Online Proceedings Library Archive*. 236. 1991.
86. Focus Technology Co L. *Mitsui Chemicals Aurum Pi Jcl3030 Polyimide Resin*. 2019.
87. Huang J-c, He C-b, Xiao Y, Mya KY, Dai J, Siow YP. Polyimide/POSS nanocomposites: interfacial interaction, thermal properties and mechanical properties. *Polymer.* 2003;44:4491–4499.
88. Numata Si, Oohara S, Fujisaki K, Imaizumi JI, Kinjo N. Thermal expansion behavior of various aromatic polyimides. *J Appl Polym Sci.* 1986;31:101–110.
89. Carlson DE, Wronski CR. Amorphous silicon solar cell. *Appl Phys Lett.* 1976;28: 671–673.
90. Nayak PK, Mahesh S, Snaith HJ, Cahen D. Photovoltaic solar cell technologies: analysing the state of the art. *Nat. Rev. Mater.* 2019;4:269–285.
91. Fritzsche H. Photo-induced structural changes associated with the Staebler-Wronski effect in hydrogenated amorphous silicon. *Solid State Commun.* 1995;94:953–955.
92. Gao X, Zhao Z. High mobility organic semiconductors for field-effect transistors. *Sci China Chem.* 2015;58:947–968.
93. Zhao L, Luo D, Zhu R. *Flexible Photovoltaic Systems. Flexible and Stretchable Medical Devices*. 2018:105–137.
94. Koh J, Lee Y, Fujiwara H, Wronski CR, Collins RW. Optimization of hydrogenated amorphous silicon p–i–n solar cells with two-step i layers guided by real-time spectroscopic ellipsometry. *Appl Phys Lett.* 1998;73:1526–1528.
95. Yang J, Banerjee A, Guha S. Triple-junction amorphous silicon alloy solar cell with 14.6% initial and 13.0% stable conversion efficiencies. *Appl Phys Lett.* 1997;70: 2975–2977.
96. Contreras MA, Mansfield LM, Egaas B, et al. Wide bandgap Cu (In, Ga) Se₂ solar cells with improved energy conversion efficiency. *Prog Photovoltaics Res Appl.* 2012; 20:843–850.
97. Feurer T, Reinhard P, Avancini E, et al. Progress in thin film CIGS photovoltaics—Research and development, manufacturing, and applications. *Prog Photovoltaics Res Appl.* 2017;25:645–667.
98. Chirilă A, Buecheler S, Pianezzi F, et al. Highly efficient Cu (In, Ga) Se₂ solar cells grown on flexible polymer films. *Nat Mater.* 2011;10:857–861.
99. Ramanujam J, Bishop DM, Todorov TK, et al. Flexible CIGS, CdTe and a-Si: H based thin film solar cells: a review. *Prog Mater Sci.* 2020;110:100619.
100. Reinhard P, Bissig B, Pianezzi F, et al. Features of KF and NaF postdeposition treatments of Cu (In, Ga) Se₂ absorbers for high efficiency thin film solar cells. *Chem Mater.* 2015;27:5755–5764.
101. Jackson P, Wuerz R, Hariskos D, Lotter E, Witte W, Powalla M. Effects of heavy alkali elements in Cu (In, Ga) Se₂ solar cells with efficiencies up to 22.6%. *Phys Status Solidi Rapid Res Lett.* 2016;10:583–586.
102. Li Y, Xu G, Cui C, Li Y. Flexible and semitransparent organic solar cells. *Adv Energy Mater.* 2018;8:1701791.
103. Xu X, Sun L, Shen K, Zhang S. Organic and hybrid organic-inorganic flexible optoelectronics: recent advances and perspectives. *Synth Met.* 2019;256:116137.
104. Zhang F, Inganäs O, Zhou Y, Vandewal K. Development of polymer–fullerene solar cells. *Nat Sci Rev.* 2016;3:222–239.
105. Yeh N, Yeh P. Organic solar cells: their developments and potentials. *Renew Sustain Energy Rev.* 2013;21:421–431.
106. Beard MC, Midgett AG, Hanna MC, Luther JM, Hughes BK, Nozik AJ. Comparing multiple exciton generation in quantum dots to impact ionization in bulk semiconductors: implications for enhancement of solar energy conversion. *Nano Lett.* 2010;10:3019–3027.
107. Beard MC, Midgett AG, Law M, Semonin OE, Ellingson RJ, Nozik AJ. Variations in the quantum efficiency of multiple exciton generation for a series of chemically treated PbSe nanocrystal films. *Nano Lett.* 2009;9:836–845.
108. Li P, Lu ZH, Lu ZH. *Heterojunction Energetics and Open-Circuit Voltages of Organic Photovoltaic Cells. Emerging Photovoltaic Materials: Silicon & beyond*. 2018:487–510.
109. Cheng P, Zhan X. Stability of organic solar cells: challenges and strategies. *Chem Soc Rev.* 2016;45:2544–2582.
110. Wang K, Liu C, Meng T, Yi C, Gong X. Inverted organic photovoltaic cells. *Chem Soc Rev.* 2016;45:2937–2975.
111. Lloyd MT, Peters CH, Garcia A, et al. Influence of the hole-transport layer on the initial behavior and lifetime of inverted organic photovoltaics. *Sol Energy Mater Sol Cells.* 2011;95:1382–1388.
112. Choy WC, Zhang D. Solution-processed metal oxides as efficient carrier transport layers for organic photovoltaics. *Small.* 2012;12:416–431.
113. Hau SK, Yip H-L, Leong K, Jen AK-Y. Spraycoating of silver nanoparticle electrodes for inverted polymer solar cells. *Org Electron.* 2009;10:719–723.
114. Krebs FC, Gevorgyan SA, Alstrup J. A roll-to-roll process to flexible polymer solar cells: model studies, manufacture and operational stability studies. *J Mater Chem.* 2009;19:5442–5451.
115. Lloyd MT, Olson DC, Lu P, et al. Impact of contact evolution on the shelf life of organic solar cells. *J Mater Chem.* 2009;19:7638–7642.
116. Svensson M, Zhang F, Veenstra SC, et al. High-performance polymer solar cells of an alternating polyfluorene copolymer and a fullerene derivative. *Adv Mater.* 2003;15: 988–991.
117. Inganäs O, Svensson M, Zhang F, et al. Low bandgap alternating polyfluorene copolymers in plastic photodiodes and solar cells. *Appl Phys A.* 2004;79:31–35.
118. Zhang F, Perzon E, Wang X, Mammo W, Andersson MR, Inganäs O. Polymer solar cells based on a low-bandgap fluorene copolymer and a fullerene derivative with photocurrent extended to 850 nm. *Adv Funct Mater.* 2005;15:745–750.
119. Inganäs O, Zhang F, Tvingstedt K, Andersson LM, Hellström S, Andersson MR. Polymer photovoltaics with alternating copolymer/fullerene blends and novel device architectures. *Adv Mater.* 2010;22:E100–E116.
120. Van Duren J, Dhanabalan A, Van Hal P, Janssen R. Low-bandgap polymer photovoltaic cells. *Synth Met.* 2001;121:1587–1588.
121. Dhanabalan A, van Duren JK, van Hal PA, van Dongen JL, Janssen R. Synthesis and characterization of a low bandgap conjugated polymer for bulk heterojunction photovoltaic cells. *Adv Funct Mater.* 2001;11:255–262.
122. Neugebauer H, Kvarnström C, Brabec C, et al. Infrared spectroelectrochemical investigations on the doping of soluble poly (isothianaphthene methine)(PIM). *J Chem Phys.* 1999;110:12108–12115.
123. Scharber MC, Mühlbacher D, Koppe M, et al. Design rules for donors in bulk-heterojunction solar cells—towards 10% energy-conversion efficiency. *Adv Mater.* 2006;18:789–794.
124. Li L, Counts KE, Kurosawa S, Teja AS, Collard DM. Tuning the electronic structure and solubility of conjugated polymers with perfluoroalkyl substituents: poly (3-perfluorooctylthiophene), the first supercritical CO₂-soluble conjugated polymer. *Adv Mater.* 2004;16:180–183.
125. Ismail YA, Soga T, Jimbo T. Improvement in light harvesting and performance of P3HT: PCBM solar cell by using 9, 10-diphenylanthracene. *Sol Energy Mater Sol Cells.* 2009;93:1582–1586.
126. Rand BP, Xue J, Yang F, Forrest SR. Organic solar cells with sensitivity extending into the near infrared. *Appl Phys Lett.* 2005;87:233508.

127. Ingram GL, Nguyen C, Lu Z-H. Long-range energy transfer and singlet-exciton migration in working organic light-emitting diodes. *Phys Rev Appl.* 2016;5:064002.
128. Markov DE, Amsterdam E, Blom PW, Sieval AB, Hummelen JC. Accurate measurement of the exciton diffusion length in a conjugated polymer using a heterostructure with a side-chain cross-linked fullerene layer. *J Phys Chem.* 2005; 109:5266–5274.
129. Markov D, Tanase C, Blom P, Wildeman J. Simultaneous enhancement of charge transport and exciton diffusion in poly (p-phenylene vinylene) derivatives. *Phys Rev B.* 2005;72:045217.
130. Granström M, Petritsch K, Arias A, Lux A, Andersson M, Friend R. Laminated fabrication of polymeric photovoltaic diodes. *Nature.* 1998;395:257.
131. Rand BP, Schols S, Cheyns D, et al. Organic solar cells with sensitized phosphorescent absorbing layers. *Org Electron.* 2009;10:1015–1019.
132. Heremans P, Cheyns D, Rand BP. Strategies for increasing the efficiency of heterojunction organic solar cells: material selection and device architecture. *Acc Chem Res.* 2009;42:1740–1747.
133. Rand BP, Genoe J, Heremans P, Poortmans J. Solar cells utilizing small molecular weight organic semiconductors. *Prog Photovoltaics Res Appl.* 2007;15:659–676.
134. Thompson BC, Fréchet JM. Polymer–fullerene composite solar cells. *Angew Chem Int Ed.* 2008;47:58–77.
135. Dennler G, Scharber MC, Brabec CJ. Polymer–fullerene bulk-heterojunction solar cells. *Adv Mater.* 2009;21:1323–1338.
136. Burlingame Q, Coburn C, Che X, Panda A, Qu Y, Forrest SR. Centimetre-scale electron diffusion in photoactive organic heterostructures. *Nature.* 2018;554:77.
137. Vandewal K, Tvingstedt K, Gadisa A, Inganäs O, Manca JV. On the origin of the open-circuit voltage of polymer–fullerene solar cells. *Nat Mater.* 2009;8:904.
138. Brabec CJ, Cravino A, Meissner D, et al. Origin of the open circuit voltage of plastic solar cells. *Adv Funct Mater.* 2001;11:374–380.
139. Tang C, Albrecht A. Photovoltaic effects of metal–chlorophyll-a–metal sandwich cells. *J Chem Phys.* 1975;62:2139–2149.
140. Tang CW. Two-layer organic photovoltaic cell. *Appl Phys Lett.* 1986;48:183–185.
141. Al-Ibrahim M, Roth HK, Sensfuss S. Efficient large-area polymer solar cells on flexible substrates. *Appl Phys Lett.* 2004;85:1481–1483.
142. Lungenschmied C, Dennler G, Neugebauer H, et al. Flexible, long-lived, large-area, organic solar cells. *Sol Energy Mater Sol Cells.* 2007;91:379–384.
143. Peet J, Kim JY, Coates NE, et al. Efficiency enhancement in low-bandgap polymer solar cells by processing with alkane dithiols. *Nat Mater.* 2007;6:497.
144. Park Y-S, Choi K-H, Kim H-K. Room temperature flexible and transparent ITO/Ag/ITO electrode grown on flexible PES substrate by continuous roll-to-roll sputtering for flexible organic photovoltaics. *J Phys D Appl Phys.* 2009;42:235109.
145. Wang J-C, Weng W-T, Tsai M-Y, et al. Highly efficient flexible inverted organic solar cells using atomic layer deposited ZnO as electron selective layer. *J Mater Chem.* 2010;20:862–866.
146. Sun Y, Welch GC, Leong WL, Takacs CJ, Bazan GC, Heeger AJ. Solution-processed small-molecule solar cells with 6.7% efficiency. *Nat Mater.* 2012;11:44.
147. Wei G, Wang S, Sun K, Thompson ME, Forrest SR. Solvent-Annealed crystalline squaraine: PC70BM (1: 6) solar Cells. *Adv Energy Mater.* 2011;1:184–187.
148. Van Der Poll TS, Love JA, Nguyen TQ, Bazan GC. Non-basic high-performance molecules for solution-processed organic solar cells. *Adv Mater.* 2012;24: 3646–3649.
149. Kyaw AKK, Wang DH, Gupta V, et al. Efficient solution-processed small-molecule solar cells with inverted structure. *Adv Mater.* 2013;25:2397–2402.
150. Yao K, Xin XK, Chueh CC, Chen KS, Xu YX, Jen AKY. Enhanced light-harvesting by integrating synergetic microcavity and plasmonic effects for high-performance ITO-free flexible polymer solar cells. *Adv Funct Mater.* 2015;25:567–574.
151. Zhao B, He Z, Cheng X, et al. Flexible polymer solar cells with power conversion efficiency of 8.7%. *J Mater Chem C.* 2014;2:5077–5082.
152. Cnops K, Rand BP, Cheyns D, Verreert B, Empl MA, Heremans P. 8.4% efficient fullerene-free organic solar cells exploiting long-range exciton energy transfer. *Nat Commun.* 2014;5:3406.
153. Zhang Q, Kan B, Liu F, et al. Small-molecule solar cells with efficiency over 9%. *Nat Photon.* 2015;9:35.
154. Xue Z, Liu X, Zhang N, et al. High-performance NiO/Ag/NiO transparent electrodes for flexible organic photovoltaic cells. *ACS Appl Mater Interfaces.* 2014;6: 16403–16408.
155. Zou J, Li CZ, Chang CY, Yip HL, Jen AKY. Interfacial engineering of ultrathin metal film transparent electrode for flexible organic photovoltaic cells. *Adv Mater.* 2014; 26:3618–3623.
156. Berny S, Blouin N, Distler A, et al. Solar trees: first large-scale demonstration of fully solution coated, semitransparent, flexible organic photovoltaic modules. *Adv Sci.* 2016;3:1500342.
157. Kim Y, Ryu TI, Ok KH, et al. Inverted layer-by-layer fabrication of an ultraflexible and transparent Ag nanowire/conductive polymer composite electrode for use in high-performance organic solar cells. *Adv Funct Mater.* 2015;25:4580–4589.
158. Lin Y, Wang J, Zhang ZG, et al. An electron acceptor challenging fullerenes for efficient polymer solar cells. *Adv Mater.* 2015;27:1170–1174.
159. Zhong Y, Trinh MT, Chen R, et al. Molecular helices as electron acceptors in high-performance bulk heterojunction solar cells. *Nat Commun.* 2015;6:8242.
160. Huang J, Li CZ, Chueh CC, Liu SQ, Yu JS, Jen AKY. 10.4% power conversion efficiency of ITO-free organic photovoltaics through enhanced light trapping configuration. *Adv Energy Mater.* 2015;5:1500406.
161. Kang H, Jung S, Jeong S, Kim G, Lee K. Polymer-metal hybrid transparent electrodes for flexible electronics. *Nat Commun.* 2015;6:6503.
162. Kan B, Li M, Zhang Q, et al. A series of simple oligomer-like small molecules based on oligothiophenes for solution-processed solar cells with high efficiency. *J Am Chem Soc.* 2015;137:3886–3893.
163. Park Y, Nehm F, Mueller-Meskamp L, Vandewal K, Leo K. Optical display film as flexible and light trapping substrate for organic photovoltaics. *Optic Express.* 2016; 24:A974–A980.
164. Lin Y, Zhao F, He Q, et al. High-performance electron acceptor with thienyl side chains for organic photovoltaics. *J Am Chem Soc.* 2016;138:4955–4961.
165. Li S, Ye L, Zhao W, et al. Energy-level modulation of small-molecule electron acceptors to achieve over 12% efficiency in polymer solar cells. *Adv Mater.* 2016;28: 9423–9429.
166. Wang J-L, Liu K-K, Yan J, et al. Series of multifluorine substituted oligomers for organic solar cells with efficiency over 9% and fill factor of 0.77 by combination thermal and solvent vapor annealing. *J Am Chem Soc.* 2016;138:7687–7697.
167. Chen S, Liu Y, Zhang L, et al. A wide-bandgap donor polymer for highly efficient non-fullerene organic solar cells with a small voltage loss. *J Am Chem Soc.* 2017; 139:6298–6301.
168. Zhao W, Li S, Yao H, et al. Molecular optimization enables over 13% efficiency in organic solar cells. *J Am Chem Soc.* 2017;139:7148–7151.
169. Li S, Ye L, Zhao W, et al. A wide band gap polymer with a deep highest occupied molecular orbital level enables 14.2% efficiency in polymer solar cells. *J Am Chem Soc.* 2018;140:7159–7167.
170. Qiu B, Xue L, Yang Y, et al. All-small-molecule nonfullerene organic solar cells with high fill factor and high efficiency over 10%. *Chem Mater.* 2017;29:7543–7553.
171. Xu G, Shen L, Cui C, et al. High-performance colorful semitransparent polymer solar cells with ultrathin hybrid-metal electrodes and fine-tuned dielectric mirrors. *Adv Funct Mater.* 2017;27:1605908.
172. Zhang J, Xue R, Xu G, et al. Self-doping fullerene electrolyte-based electron transport layer for all-room-temperature-processed high-performance flexible polymer solar cells. *Adv Funct Mater.* 2018;28:1705847.
173. Park S, Heo SW, Lee W, et al. Self-powered ultra-flexible electronics via nano-grating-patterned organic photovoltaics. *Nature.* 2018;561:516.
174. Xu X, Fukuda K, Karki A, et al. Thermally stable, highly efficient, ultraflexible organic photovoltaics. *Proc Natl Acad Sci Unit States Am.* 2018;115:4589–4594.
175. Li H, Xiao Z, Ding L, Wang J. Thermostable single-junction organic solar cells with a power conversion efficiency of 14.62%. *Sci Bull.* 2018;63:340–342.
176. Zhang S, Qin Y, Zhu J, Hou J. Over 14% efficiency in polymer solar cells enabled by a chlorinated polymer donor. *Adv Mater.* 2018;30:1800868.
177. Sun Y, Chang M, Meng L, et al. Flexible organic photovoltaics based on water-processed silver nanowire electrodes. *Na Electronics.* 2019;2:513–520.
178. Yan T, Song W, Huang J, Peng R, Huang L, Ge Z. 16.67% rigid and 14.06% flexible organic solar cells enabled by ternary heterojunction strategy. *Adv Mater.* 2019; 31(39):1902210.
179. Cui Y, Yao H, Hong L, et al. Achieving over 15% efficiency in organic photovoltaic cells via copolymer design. *Adv Mater.* 2019;31:1808356.
180. Zhou R, Jiang Z, Yang C, et al. All-small-molecule organic solar cells with over 14% efficiency by optimizing hierarchical morphologies. *Nat Commun.* 2019;10:1–9.
181. Yuan J, Zhang Y, Zhou L, et al. Single-junction organic solar cell with over 15% efficiency using fused-ring acceptor with electron-deficient core. *Joule.* 2019;3: 1140–1151.
182. Cui Y, Yao H, Zhang J, et al. Over 16% efficiency organic photovoltaic cells enabled by a chlorinated acceptor with increased open-circuit voltages. *Nat Commun.* 2019; 10:2515.
183. Chen X, Xu G, Zeng G, et al. Realizing ultrahigh mechanical flexibility and > 15% efficiency of flexible organic solar cells via a “welding” flexible transparent electrode. *Adv Mater.* 2020;32:1908478.
184. Qin J, Zhang L, Xiao Z, Chen S, Sun K, Zhang Z, Yi C, Yuan Y, Jin Z, Hao F. Over 16% efficiency from thick-film organic solar cells. *Sci Bull.* 2020. https://www.researchgate.net/profile/Zuo_Xiao2/publication/343874288_Over_16_efficiency_from_thick-film_organic_solar_cells/links/5f52eed192851c250b9268bb/Over-16-efficiency-from-thick-film-organic-solar-cells.pdf.
185. Docampo P, Ball JM, Darwich M, Eperon GE, Snaith HJ. Efficient organometal trihalide perovskite planar-heterojunction solar cells on flexible polymer substrates. *Nat Commun.* 2013;4:2761.
186. Green MA, Ho-Baillie A, Snaith HJ. The emergence of perovskite solar cells. *Nat Photon.* 2014;8:506–514.
187. Stranks SD, Hoyer RLZ, Di D, Friend RH, Deschler F. The physics of light emission in halide perovskite devices. *Adv Mater.* 2018, e1803336.
188. Wang Y, Bai S, Cheng L, et al. High-efficiency flexible solar cells based on organometal halide perovskites. *Adv Mater.* 2016;28:4532–4540.
189. Palmstrom AF, Eperon GE, Leijtens T, et al. Enabling flexible all-perovskite tandem solar cells. *Joule.* 2019;3:2193–2204.
190. Najafi M, Di Giacomo F, Zhang D, et al. Highly efficient and stable flexible perovskite solar cells with metal oxides nanoparticle charge extraction layers. *Small.* 2018;14, e1702775.
191. Tao S, Schmidt I, Brocks G, et al. Absolute energy level positions in tin- and lead-based halide perovskites. *Nat Commun.* 2019;10:2560.
192. Snaith HJ. Perovskites: the emergence of a new era for low-cost, high-efficiency solar cells. *J Phys Chem Lett.* 2013;4:3623–3630.
193. Eperon GE, Hörantner MT, Snaith HJ. Metal halide perovskite tandem and multiple-junction photovoltaics. *Nat RevChem.* 2017;1.
194. Yang D, Yang R, Wang K, et al. High efficiency planar-type perovskite solar cells with negligible hysteresis using EDTA-complexed SnO₂. *Nat Commun.* 2018;9: 1–11.
195. Najafi M, Di Giacomo F, Zhang D, et al. Highly efficient and stable flexible perovskite solar cells with metal oxides nanoparticle charge extraction layers. *Small.* 2018;14:1702775.

196. Liu C, Zhang L, Zhou X, et al. Hydrothermally treated SnO₂ as the electron transport layer in high-efficiency flexible perovskite solar cells with a certificated efficiency of 17.3%. *Adv Funct Mater.* 2019;29:1807604.
197. Palmstrom AF, Eperon GE, Leijtens T, et al. Enabling flexible all-perovskite tandem solar cells. *Joule.* 2019;3:2193–2204.
198. Kim BJ, Kim DH, Lee Y-Y, et al. Highly efficient and bending durable perovskite solar cells: toward a wearable power source. *Energy Environ Sci.* 2015;8:916–921.
199. Li Y, Meng L, Yang YM, et al. High-efficiency robust perovskite solar cells on ultrathin flexible substrates. *Nat Commun.* 2016;7:1–10.
200. Abdi-Jalebi M, Andaji-Garmaroudi Z, Cacovich S, et al. Maximizing and stabilizing luminescence from halide perovskites with potassium passivation. *Nature.* 2018; 555:497–501.
201. Kaltenbrunner M, Adam G, Glowacki ED, et al. Flexible high power-per-weight perovskite solar cells with chromium oxide-metal contacts for improved stability in air. *Nat Mater.* 2015;14:1032–1039.
202. Chen W, Sun H, Hu Q, et al. High short-circuit current density via integrating the perovskite and ternary organic bulk heterojunction. *ACS Energy Lett.* 2019;4: 2535–2536.
203. Yuan J, Zhang Y, Zhou L, et al. Single-junction organic solar cell with over 15% efficiency using fused-ring acceptor with electron-deficient core. *Joule.* 2019;3: 1140–1151.
204. Tu Y, Xu G, Yang X, et al. Mixed-cation perovskite solar cells in space. *Sci China Phys Mech Astron.* 2019;62.
205. Matsui T, Bidiville A, Maejima K, et al. High-efficiency amorphous silicon solar cells: impact of deposition rate on metastability. *Appl Phys Lett.* 2015;106, 053901.
206. Hedler A, Klaumunzer SL, Wesch W. Amorphous silicon exhibits a glass transition. *Nat Mater.* 2004;3:804–809.
207. Zhou H, Chen Q, Li G, et al. Photovoltaics. Interface engineering of highly efficient perovskite solar cells. *Science.* 2014;345:542–546.
208. Stranks SD, Eperon GE, Grancini G, et al. Electron-hole diffusion lengths exceeding 1 micrometer in an organometal trihalide perovskite absorber. *Science.* 2013;342: 341–344.
209. Zhao L, Luo D, Wu J, et al. High-performance inverted planar heterojunction perovskite solar cells based on lead acetate precursor with efficiency exceeding 18%. *Adv Funct Mater.* 2016;26:3508–3514.
210. Lim J, Hörantner MT, Sakai N, et al. Elucidating the long-range charge carrier mobility in metal halide perovskite thin films. *Energy Environ Sci.* 2019;12:169–176.
211. Zhang W, Saliba M, Moore DT, et al. Ultrasoft organic-inorganic perovskite thin-film formation and crystallization for efficient planar heterojunction solar cells. *Nat Commun.* 2015;6:6142.
212. Eperon GE, Stranks SD, Menelaou C, Johnston MB, Herz LM, Snaith HJ. Formamidinium lead trihalide: a broadly tunable perovskite for efficient planar heterojunction solar cells. *Energy Environ Sci.* 2014;7:982.
213. Jeon NJ, Noh JH, Yang WS, et al. Compositional engineering of perovskite materials for high-performance solar cells. *Nature.* 2015;517:476–480.
214. Wang Y, Dar MI, Ono LK, et al. Thermodynamically stabilized beta-CsPbI₃-based perovskite solar cells with efficiencies >18. *Science.* 2019;365:591–595.
215. Wang Y, Zhang T, Kan M, Zhao Y. Bifunctional stabilization of all-inorganic alpha-CsPbI₃ perovskite for 17% efficiency photovoltaics. *J Am Chem Soc.* 2018;140: 12345–12348.
216. Steele JA, Jin H, Dovgaliuk I, et al. Thermal nonequilibrium of strained black CsPbI₃ thin films. *Science.* 2019;365:679–684.
217. Jiang Q, Zhao Y, Zhang X, et al. Surface passivation of perovskite film for efficient solar cells. *Nat Photon.* 2019;13:460–466.
218. Jeon NJ, Na H, Jung EH, et al. A fluorene-terminated hole-transporting material for highly efficient and stable perovskite solar cells. *Nat Energy.* 2018;3:682–689.
219. Wang Z, Lin Q, Chmiel FP, Sakai N, Herz LM, Snaith HJ. Efficient ambient-air-stable solar cells with 2D–3D heterostructured butylammonium-caesium-formamidinium lead halide perovskites. *Nat Energy.* 2017;2.
220. Bai S, Da P, Li C, et al. Planar perovskite solar cells with long-term stability using ionic liquid additives. *Nature.* 2019;571:245–250.
221. Saliba M, Matsui T, Seo JY, et al. Cesium-containing triple cation perovskite solar cells: improved stability, reproducibility and high efficiency. *Energy Environ Sci.* 2016;9:1989–1997.
222. Zheng X, Chen B, Dai J, et al. Defect passivation in hybrid perovskite solar cells using quaternary ammonium halide anions and cations. *Nat Energy.* 2017;2.
223. Tan H, Jain A, Voznyy O, et al. Efficient and stable solution-processed planar perovskite solar cells via contact passivation. *Science.* 2017;355:722–726.
224. Wang Z, Lin Q, Wenger B, et al. High irradiance performance of metal halide perovskites for concentrator photovoltaics. *Nat Energy.* 2018;3:855–861.
225. Saliba M, Matsui T, Domanski K, et al. Incorporation of rubidium cations into perovskite solar cells improves photovoltaic performance. *Science.* 2016;354:206–209.
226. Correa-Baena JP, Luo Y, Brenner TM, et al. Homogenized halides and alkali cation segregation in alloyed organic-inorganic perovskites. *Science.* 2019;363:627–631.
227. Lin R, Xiao K, Qin Z, et al. Monolithic all-perovskite tandem solar cells with 24.8% efficiency exploiting comproportionation to suppress Sn(II) oxidation in precursor ink. *Nat Energy.* 2019;4:864–873.
228. Ke W, Kanatzidis MG. Prospects for low-toxicity lead-free perovskite solar cells. *Nat Commun.* 2019;10:965.
229. Tang CW, VanSlyke SA. Organic electroluminescent diodes. *Appl Phys Lett.* 1987;51: 913–915.
230. Xue J, Forrest SR. Carrier transport in multilayer organic photodetectors: II. Effects of anode preparation. *J Appl Phys.* 2004;95:1869–1877.
231. Milliron D, Hill I, Shen C, Kahn A, Schwartz J. Surface oxidation activates indium tin oxide for hole injection. *J Appl Phys.* 2000;87:572–576.
232. Li C, Kwong C, Djurišić A, et al. Improved performance of OLEDs with ITO surface treatments. *Thin Solid Films.* 2005;477:57–62.
233. Hong Z, Liang C, Sun X, Zeng X. Characterization of organic photovoltaic devices with indium-tin-oxide anode treated by plasma in various gases. *J Appl Phys.* 2006; 100, 093711.
234. Destruel P, Bock H, Séguin I, Jolinat P, Oukachmih M, Bedel-Pereira E. Influence of indium tin oxide treatment using UV-ozone and argon plasma on the photovoltaic parameters of devices based on organic discotic materials. *Polym Int.* 2006;55: 601–607.
235. Helander M, Wang Z, Qiu J, et al. Chlorinated indium tin oxide electrodes with high work function for organic device compatibility. *Science.* 2011;332:944–947.
236. Huang J-H, Kekuda D, Chu C-W, Ho K-C. Electrochemical characterization of the solvent-enhanced conductivity of poly (3, 4-ethylenedioxythiophene) and its application in polymer solar cells. *J Mater Chem.* 2009;19:3704–3712.
237. Peng B, Guo X, Cui C, Zou Y, Pan C, Li Y. Performance improvement of polymer solar cells by using a solvent-treated poly (3, 4-ethylenedioxythiophene): poly (styrenesulfonate) buffer layer. *Appl Phys Lett.* 2011;98:113.
238. Irwin MD, Servaites JD, Buchholz DB, et al. Structural and electrical functionality of NiO interfacial films in bulk heterojunction organic solar cells. *Chem Mater.* 2011; 23:2218–2226.
239. Hammond SR, Meyer J, Widjono NE, et al. Low-temperature, solution-processed molybdenum oxide hole-collection layer for organic photovoltaics. *J Mater Chem.* 2012;22:3249–3254.
240. Meyer J, Hamwi S, Kröger M, Kowalsky W, Riedl T, Kahn A. Transition metal oxides for organic electronics: energetics, device physics and applications. *Adv Mater.* 2012;24:5408–5427.
241. Manders JR, Tsang SW, Hartel MJ, et al. Solution-processed nickel oxide hole transport layers in high efficiency polymer photovoltaic cells. *Adv Funct Mater.* 2013;23:2993–3001.
242. Waldauf C, Morana M, Denk P, et al. Highly efficient inverted organic photovoltaics using solution based titanium oxide as electron selective contact. *Appl Phys Lett.* 2006;89:233517.
243. Hau SK, Yip H-L, Baek NS, Zou J, O'Malley K, Jen AK-Y. Air-stable inverted flexible polymer solar cells using zinc oxide nanoparticles as an electron selective layer. *Appl Phys Lett.* 2008;92:225.
244. Qian L, Yang J, Zhou R, et al. Hybrid polymer-CdSe solar cells with a ZnO nanoparticle buffer layer for improved efficiency and lifetime. *J Mater Chem.* 2011; 21:3814–3817.
245. Sun Y, Seo JH, Takacs CJ, Seifter J, Heeger AJ. Inverted polymer solar cells integrated with a low-temperature-annealed sol-gel-derived ZnO film as an electron transport layer. *Adv Mater.* 2011;23:1679–1683.
246. Zhou R, Zheng Y, Qian L, Yang Y, Holloway PH, Xue J. Solution-processed, nanostructured hybrid solar cells with broad spectral sensitivity and stability. *Nanoscale.* 2012;4:3507–3514.
247. Hecht DS, Hu L, Irvin G. Emerging transparent electrodes based on thin films of carbon nanotubes, graphene, and metallic nanostructures. *Adv Mater.* 2011;23: 1482–1513.
248. Krantz J, Richter M, Spallek S, Spiecker E, Brabec CJ. Solution-processed metallic nanowire electrodes as indium tin oxide replacement for thin-film solar cells. *Adv Funct Mater.* 2011;21:4784–4787.
249. Sandström A, Dam HF, Krebs FC, Edman L. Ambient fabrication of flexible and large-area organic light-emitting devices using slot-die coating. *Nat Commun.* 2012; 3:1002.
250. Na SI, Kim SS, Jo J, Kim DY. Efficient and flexible ITO-free organic solar cells using highly conductive polymer anodes. *Adv Mater.* 2008;20:4061–4067.
251. Kim KS, Zhao Y, Jang H, et al. Large-scale pattern growth of graphene films for stretchable transparent electrodes. *Nature.* 2009;457:706.
252. Gupta D, Wienk MM, Janssen RAJ. Efficient polymer solar cells on opaque substrates with a laminated PEDOT:PSS top electrode. *Adv Energy Mater.* 2013;3: 782–787.
253. Liu H, Wu Z, Hu J, et al. Efficient and ultraviolet durable inverted organic solar cells based on an aluminum-doped zinc oxide transparent cathode. *Appl Phys Lett.* 2013; 103:135,131.
254. Park J-H, Ahn K-J, Na S-I, Kim H-K. Effects of deposition temperature on characteristics of Ga-doped ZnO film prepared by highly efficient cylindrical rotating magnetron sputtering for organic solar cells. *Sol Energy Mater Sol Cells.* 2011;95:657–663.
255. Murdoch G, Hinds S, Sargent E, Tsang S, Mordoukhovskii L, Lu Z. Aluminum doped zinc oxide for organic photovoltaics. *Appl Phys Lett.* 2009;94:138.
256. Fortunato E, Ginley D, Hosono H, Paine DC. Transparent conducting oxides for photovoltaics. *MRS Bull.* 2007;32:242–247.
257. Park SH, Park JB, Song PK. Characteristics of Al-doped, Ga-doped and In-doped zinc-oxide films as transparent conducting electrodes in organic light-emitting diodes. *Curr Appl Phys.* 2010;10:S488–S490.
258. Wang Z, Helander M, Lu Z. Transparent conducting thin films for OLEDs. In: *Organic Light-Emitting Diodes (OLEDs)*. Elsevier; 2013:49–76.
259. Pöde R, Lee C, Moon D, Han J. Transparent conducting metal electrode for top emission organic light-emitting devices: Ca-Ag double layer. *Appl Phys Lett.* 2004; 84:4614–4616.
260. Al-Ibrahim M, Sensfuss S, Uziel J, Ecke G, Ambacher O. Comparison of normal and inverse poly (3-hexylthiophene)/fullerene solar cell architectures. *Sol Energy Mater Sol Cell.* 2005;85:277–283.
261. Bailey-Salzman RF, Rand BP, Forrest SR. Semitransparent organic photovoltaic cells. *Appl Phys Lett.* 2006;88:233502.
262. O'Connor B, Haughn C, An K-H, Pipe KP, Shtein M. Transparent and conductive electrodes based on unpatterned, thin metal films. *Appl Phys Lett.* 2008;93:433.

263. Wilken S, Hoffmann T, Von Hauff E, Borchert H, Parisi J. ITO-free inverted polymer/fullerene solar cells: interface effects and comparison of different semi-transparent front contacts. *Sol Energy Mater Sol Cell*. 2012;96:141–147.
264. Chen K-S, Salinas J-F, Yip H-L, Huo L, Hou J, Jen AK-Y. Semi-transparent polymer solar cells with 6% PCE, 25% average visible transmittance and a color rendering index close to 100 for power generating window applications. *Energy Environ Sci*. 2012;5:9551–9557.
265. Fan JC, Bachner FJ, Foley GH, Zavracky PM. Transparent heat-mirror films of TiO₂/Ag/TiO₂ for solar energy collection and radiation insulation. *Appl Phys Lett*. 1974;25:693–695.
266. Cattin L, Morsli M, Dahou F, Abe SY, Khelil A, Bernède J. Investigation of low resistance transparent MoO₃/Ag/MoO₃ multilayer and application as anode in organic solar cells. *Thin Solid Films*. 2010;518:4560–4563.
267. Choa S-H, Cho C-K, Hwang W-J, Eun KT, Kim H-K. Mechanical integrity of flexible InZnO/Ag/InZnO multilayer electrodes grown by continuous roll-to-roll sputtering. *Sol Energy Mater Sol Cells*. 2011;95:3442–3449.
268. Hong K, Kim K, Kim S, et al. Optical properties of WO₃/Ag/WO₃ multilayer as transparent cathode in top-emitting organic light emitting diodes. *J Phys Chem C*. 2011;115:3453–3459.
269. Cho H, Yun C, Park J-W, Yoo S. Highly flexible organic light-emitting diodes based on ZnS/Ag/WO₃ multilayer transparent electrodes. *Org Electron*. 2009;10:1163–1169.
270. Jung GH, Hong K, Dong WJ, Kim S, Lee JL. BCP/Ag/MoO₃ transparent cathodes for organic photovoltaics. *Adv Energy Mater*. 2011;1:1023–1028.
271. Lim S, Han D, Kim H, Lee S, Yoo S. Cu-based multilayer transparent electrodes: a low-cost alternative to ITO electrodes in organic solar cells. *Sol Energy Mater Sol Cells*. 2012;101:170–175.
272. Yu J-S, Jung GH, Jo J, et al. Transparent conductive film with printable embedded patterns for organic solar cells. *Sol Energy Mater Sol Cells*. 2013;109:142–147.
273. Zou J, Yip H-L, Hau SK, Jen AK-Y. Metal grid/conducting polymer hybrid transparent electrode for inverted polymer solar cells. *Appl Phys Lett*. 2010;96:96.
274. Kang MG, Xu T, Park HJ, Luo X, Guo LJ. Efficiency enhancement of organic solar cells using transparent plasmonic Ag nanowire electrodes. *Adv Mater*. 2010;22:4378–4383.
275. Ho Y-H, Chen K-Y, Liu S-W, Chang Y-T, Huang D-W, Wei P-K. Transparent and conductive metallic electrodes fabricated by using nanosphere lithography. *Org Electron*. 2011;12:961–965.
276. Li Y, Mao L, Gao Y, et al. ITO-free photovoltaic cell utilizing a high-resolution silver grid current collecting layer. *Sol Energy Mater Sol Cells*. 2013;113:85–89.
277. Mao L, Chen Q, Li Y, et al. Flexible silver grid/PEDOT: PSS hybrid electrodes for large area inverted polymer solar cells. *Nano Energy*. 2014;10:259–267.
278. Lee HB, Jin W-Y, Ovhal MM, Kumar N, Kang J-W. Flexible transparent conducting electrodes based on metal meshes for organic optoelectronic device applications: a review. *J Mater Chem C*. 2019;7:1087–1110.
279. Kang MG, Kim MS, Kim J, Guo LJ. Organic solar cells using nanoimprinted transparent metal electrodes. *Adv Mater*. 2008;20:4408–4413.
280. Cao W, Li J, Chen H, Xue J. Transparent electrodes for organic optoelectronic devices: a review. *J Photon Energy*. 2014;4, 040990.
281. Zeng G, Zhang J, Chen X, Gu H, Li Y, Li Y. Breaking 12% efficiency in flexible organic solar cells by using a composite electrode. *Sci China Chem*. 2019;62:851–858.
282. Rathmell AR, Wiley BJ. The synthesis and coating of long, thin copper nanowires to make flexible, transparent conducting films on plastic substrates. *Adv Mater*. 2011;23:4798–4803.
283. Zhang D, Wang R, Wen M, et al. Synthesis of ultralong copper nanowires for high-performance transparent electrodes. *J Am Chem Soc*. 2012;134:14283–14286.
284. Belenkova TL, Rimmerman D, Mentovich E, et al. UV induced formation of transparent Au–Ag nanowire mesh film for repairable OLED devices. *J Mater Chem*. 2012;22:24042–24047.
285. Sánchez-Iglesias A, Rivas-Murias B, Grzelczak M, et al. Highly transparent and conductive films of densely aligned ultrathin Au nanowire monolayers. *Nano Lett*. 2012;12:6066–6070.
286. Rathmell AR, Nguyen M, Chi M, Wiley BJ. Synthesis of oxidation-resistant cupronickel nanowires for transparent conducting nanowire networks. *Nano Lett*. 2012;12:3193–3199.
287. Leem DS, Edwards A, Faist M, Nelson J, Bradley DD, De Mello JC. Efficient organic solar cells with solution-processed silver nanowire electrodes. *Adv Mater*. 2011;23:4371–4375.
288. Krantz J, Stubhan T, Richter M, et al. Spray-coated silver nanowires as top electrode layer in semitransparent P3HT: PCBM-based organic solar cell devices. *Adv Funct Mater*. 2013;23:1711–1717.
289. Reinhard M, Eckstein R, Slobodskyy A, Lemmer U, Colmann A. Solution-processed polymer-silver nanowire top electrodes for inverted semi-transparent solar cells. *Org Electron*. 2013;14:273–277.
290. Stubhan T, Krantz J, Li N, et al. High fill factor polymer solar cells comprising a transparent, low temperature solution processed doped metal oxide/metal nanowire composite electrode. *Sol Energy Mater Sol Cell*. 2012;107:248–251.
291. Yang L, Zhang T, Zhou H, Price SC, Wiley BJ, You W. Solution-processed flexible polymer solar cells with silver nanowire electrodes. *ACS Appl Mater Interfaces*. 2011;3:4075–4084.
292. Lee J-H, Shin H-S, Noh Y-J, Na S-I, Kim H-K. Brush painting of transparent PEDOT/Ag nanowire/PEDOT multilayer electrodes for flexible organic solar cells. *Sol Energy Mater Sol Cell*. 2013;114:15–23.
293. Gaynor W, Burkhard GF, McGehee MD, Peumans P. Smooth nanowire/polymer composite transparent electrodes. *Adv Mater*. 2011;23:2905–2910.
294. Morgenstern FS, Kabra D, Massip S, et al. Ag-nanowire films coated with ZnO nanoparticles as a transparent electrode for solar cells. *Appl Phys Lett*. 2011;99:242.
295. Ajuria J, Ugarte I, Cambarau W, Etxebarria I, Tena-Zaera R, Pacios R. Insights on the working principles of flexible and efficient ITO-free organic solar cells based on solution processed Ag nanowire electrodes. *Sol Energy Mater Sol Cell*. 2012;102:148–152.
296. Baughman RH, Zakhidov AA, De Heer WA. Carbon nanotubes—the route toward applications. *Science*. 2002;297:787–792.
297. Wu Z, Chen Z, Du X, et al. Transparent, conductive carbon nanotube films. *Science*. 2004;305:1273–1276.
298. Zhang M, Fang S, Zakhidov AA, et al. Strong, transparent, multifunctional, carbon nanotube sheets. *Science*. 2005;309:1215–1219.
299. Iijima S, Ichihashi T. Single-shell carbon nanotubes of 1-nm diameter. *Nature*. 1993;363:603.
300. Ago H, Petritsch K, Shaffer MS, Windle AH, Friend RH. Composites of carbon nanotubes and conjugated polymers for photovoltaic devices. *Adv Mater*. 1999;11:1281–1285.
301. Biris AR, Lupu D, Grüneis A, et al. High-quality double-walled carbon nanotubes grown by a cold-walled radio frequency chemical vapor deposition process. *Chem Mater*. 2008;20:3466–3472.
302. Gomez De Arco L, Zhang Y, Schlenker CW, Ryu K, Thompson ME, Zhou C. Continuous, highly flexible, and transparent graphene films by chemical vapor deposition for organic photovoltaics. *ACS Nano*. 2010;4:2865–2873.
303. Bae S, Kim H, Lee Y, et al. Roll-to-roll production of 30-inch graphene films for transparent electrodes. *Nat Nanotechnol*. 2010;5:574.
304. Lee S, Yeo J-S, Ji Y, et al. Flexible organic solar cells composed of P3HT: PCBM using chemically doped graphene electrodes. *Nanotechnology*. 2012;23:344013.
305. Iakovlev VY, Krasnikov DV, Khabushev EM, Kolodiazhaia JV, Nasibulin AG. Artificial neural network for predictive synthesis of single-walled carbon nanotubes by aerosol CVD method. *Carbon*. 2019;153:100–103.
306. Wu F, Wang C, Hu H-Y, et al. One-step synthesis of hierarchical metal oxide nanosheet/carbon nanotube composites by chemical vapor deposition. *J Mater Sci*. 2019;54:1291–1303.
307. Yang F, Wang X, Zhang D, et al. Chirality-specific growth of single-walled carbon nanotubes on solid alloy catalysts. *Nature*. 2014;510:522.
308. Zhang S, Kang L, Wang X, et al. Arrays of horizontal carbon nanotubes of controlled chirality grown using designed catalysts. *Nature*. 2017;543:234.
309. Liu J, Wang C, Tu X, et al. Chirality-controlled synthesis of single-wall carbon nanotubes using vapour-phase epitaxy. *Nat Commun*. 2012;3:1199.
310. Omachi H, Nakayama T, Takahashi E, Segawa Y, Itami K. Initiation of carbon nanotube growth by well-defined carbon nanorings. *Nat Chem*. 2013;5:572.
311. Yao Y, Feng C, Zhang J, Liu Z. “Cloning” of single-walled carbon nanotubes via open-end growth mechanism. *Nano Lett*. 2009;9:1673–1677.
312. Eda G, Fanchini G, Chhowalla M. Large-area ultrathin films of reduced graphene oxide as a transparent and flexible electronic material. *Nat Nanotechnol*. 2008;3:270.
313. Yin Z, Sun S, Salim T, et al. Organic photovoltaic devices using highly flexible reduced graphene oxide films as transparent electrodes. *ACS Nano*. 2010;4:5263–5268.
314. Becerril HA, Mao J, Liu Z, Stoltenberg RM, Bao Z, Chen Y. Evaluation of solution-processed reduced graphene oxide films as transparent conductors. *ACS Nano*. 2008;2:463–470.
315. Li D, Müller MB, Gilje S, Kaner RB, Wallace GG. Processable aqueous dispersions of graphene nanosheets. *Nat Nanotechnol*. 2008;3:101.
316. Tung VC, Allen MJ, Yang Y, Kaner RB. High-throughput solution processing of large-scale graphene. *Nat Nanotechnol*. 2009;4:25.
317. Po R, Carbonera C, Bernardi A, Camaioni N. The role of buffer layers in polymer solar cells. *Energy Environ Sci*. 2011;4:285–310.
318. Hau SK, Yip H-L, Zou J, Jen AK-Y. Indium tin oxide-free semi-transparent inverted polymer solar cells using conducting polymer as both bottom and top electrodes. *Org Electron*. 2009;10:1401–1407.
319. Zhou Y, Cheun H, Choi S, Potscavage Jr WJ, Fuentes-Hernandez C, Kippelen B. Indium tin oxide-free and metal-free semitransparent organic solar cells. *Appl Phys Lett*. 2010;97:223.
320. Hsiao Y-S, Chen C-P, Chao C-H, Whang W-T. All-solution-processed inverted polymer solar cells on granular surface-nickelized polyimide. *Org Electron*. 2009;10:551–561.
321. Zhang W, Zhao B, He Z, et al. High-efficiency ITO-free polymer solar cells using highly conductive PEDOT: PSS/surfactant bilayer transparent anodes. *Energy Environ Sci*. 2013;6:1956–1964.
322. Kim YH, Sachse C, Machala ML, May C, Müller-Meskamp L, Leo K. Highly conductive PEDOT: PSS electrode with optimized solvent and thermal post-treatment for ITO-free organic solar cells. *Adv Funct Mater*. 2011;21:1076–1081.
323. Nickel F, Puetz A, Reinhard M, et al. Cathodes comprising highly conductive poly(3, 4-ethylenedioxythiophene): poly(styrenesulfonate) for semi-transparent polymer solar cells. *Org Electron*. 2010;11:535–538.
324. Zhou Y, Cheun H, Choi S, Fuentes-Hernandez C, Kippelen B. Optimization of a polymer top electrode for inverted semitransparent organic solar cells. *Org Electron*. 2011;12:827–831.

325. Ouyang J, Chu CW, Chen FC, Xu Q, Yang Y. High-conductivity poly (3, 4-ethylenedioxythiophene): poly (styrene sulfonate) film and its application in polymer optoelectronic devices. *Adv Funct Mater.* 2005;15:203–208.
326. Kim J-R, Jung JH, Shin WS, So W-W, Moon S-J. Efficient TCO-free organic solar cells with modified poly (3, 4-ethylenedioxythiophene): poly (styrenesulfonate) anodes. *J Nanosci Nanotechnol.* 2011;11:326–330.
327. Hsiao Y-S, Whang W-T, Chen C-P, Chen Y-C. High-conductivity poly (3, 4-ethylenedioxythiophene): poly (styrene sulfonate) film for use in ITO-free polymer solar cells. *J Mater Chem.* 2008;18:5948–5955.
328. Admassie S, Zhang F, Manoj A, Svensson M, Andersson MR, Inganäs O. A polymer photodiode using vapour-phase polymerized PEDOT as an anode. *Sol Energy Mater Sol Cells.* 2006;90:133–141.
329. Mengistie DA, Ibrahim MA, Wang P-C, Chu C-W. Highly conductive PEDOT: PSS treated with formic acid for ITO-free polymer solar cells. *ACS Appl Mater Interfaces.* 2014;6:2292–2299.
330. Lee HJ, Park TH, Choi JH, et al. Negative mold transfer patterned conductive polymer electrode for flexible organic light-emitting diodes. *Org Electron.* 2013;14:416–422.
331. Hengst C, Menzel SB, Rane GK, et al. Mechanical properties of ZTO, ITO, and a-Si: H multilayer films for flexible thin film solar cells. *Materials.* 2017;10:245.
332. Lee BJ, Kim HJ, Jeong W-i, Kim J-J. A transparent conducting oxide as an efficient middle electrode for flexible organic tandem solar cells. *Sol Energy Mater Sol Cells.* 2010;94:542–546.
333. Nishiwaki H, Uchihashi K, Takaoka K, et al. Development of an ultralight, flexible a-Si solar cell submodule. *Sol Energy Mater Sol Cells.* 1995;37:295–306.
334. Yang R, Lee C-H, Cui B, Sazonov A. Flexible semi-transparent a-Si: H pin solar cells for functional energy-harvesting applications. *Mater Sci Eng, B.* 2018;229:1–5.
335. Feng J, Zhu X, Yang Z, et al. Record efficiency stable flexible perovskite solar cell using effective additive assistant strategy. *Adv Mater.* 2018;30:1801418.
336. Weerasinghe HC, Dkhissi Y, Scully AD, Caruso RA, Cheng Y-B. Encapsulation for improving the lifetime of flexible perovskite solar cells. *Nano Energy.* 2015;18:118–125.
337. Lang U, Naujoks N, Dual J. Mechanical characterization of PEDOT: PSS thin films. *Synth Met.* 2009;159:473–479.
338. Cao W, Zheng Y, Li Z, Wrzesniewski E, Hammond WT, Xue J. Flexible organic solar cells using an oxide/metal/oxide trilayer as transparent electrode. *Org Electron.* 2012;13:2221–2228.
339. Song M, You DS, Lim K, et al. Highly efficient and bendable organic solar cells with solution-processed silver nanowire electrodes. *Adv Funct Mater.* 2013;23:4177–4184.
340. Akter T, Kim WS. Reversibly stretchable transparent conductive coatings of spray-deposited silver nanowires. *ACS Appl Mater Interfaces.* 2012;4:1855–1859.
341. Miller MS, O'Kane JC, Niec A, Carmichael RS, Carmichael TB. Silver nanowire/optical adhesive coatings as transparent electrodes for flexible electronics. *ACS Appl Mater Interfaces.* 2013;5:10165–10172.
342. Lee M, Ko Y, Min BK, Jun Y. Silver nanowire top electrodes in flexible perovskite solar cells using titanium metal as substrate. *ChemSusChem.* 2016;9:31–35.
343. Jin W-Y, Ginting RT, Ko K-J, Kang J-W. Ultra-smooth, fully solution-processed large-area transparent conducting electrodes for organic devices. *Sci Rep.* 2016;6:36475.
344. Lee J, Kang H, Hwang J-Y, Kim SW, Baik S. Flexible photoanodes of TiO₂ particles and metallic single-walled carbon nanotubes for flexible dye-sensitized solar cells. *Carbon.* 2014;79:337–345.
345. Lee J-Y, Connor ST, Cui Y, Peumans P. Semitransparent organic photovoltaic cells with laminated top electrode. *Nano Lett.* 2010;10:1276–1279.
346. Wu J, Agrawal M, Becerril HA, et al. Organic light-emitting diodes on solution-processed graphene transparent electrodes. *ACS Nano.* 2009;4:43–48.
347. Nair RR, Blake P, Grigorenko AN, et al. Fine structure constant defines visual transparency of graphene. *Science.* 2008;320, 1308–1308.
348. Jeon I, Cui K, Chiba T, et al. Direct and dry deposited single-walled carbon nanotube films doped with MoO₃ as electron-blocking transparent electrodes for flexible organic solar cells. *J Am Chem Soc.* 2015;137:7982–7985.
349. Minami T. Transparent conducting oxide semiconductors for transparent electrodes. *Semicond Sci Technol.* 2005;20: S35.
350. Irfan I, Graber S, So F, Gao Y. Interplay of cleaning and de-doping in oxygen plasma treated high work function indium tin oxide (ITO). *Org Electron.* 2012;13:2028–2034.
351. Garnett EC, Cai W, Cha JJ, et al. Self-limited plasmonic welding of silver nanowire junctions. *Nat Mater.* 2012;11:241.
352. Tokuno T, Nogi M, Karakawa M, et al. Fabrication of silver nanowire transparent electrodes at room temperature. *Nano Research.* 2011;4:1215–1222.
353. Zeng XY, Zhang QK, Yu RM, Lu CZ. A new transparent conductor: silver nanowire film buried at the surface of a transparent polymer. *Adv Mater.* 2010;22:4484–4488.
354. De S, Higgins TM, Lyons PE, et al. Silver nanowire networks as flexible, transparent, conducting films: extremely high DC to optical conductivity ratios. *ACS Nano.* 2009;3:1767–1774.
355. Zhu R, Chung C-H, Cha KC, et al. Fused silver nanowires with metal oxide nanoparticles and organic polymers for highly transparent conductors. *ACS Nano.* 2011;5:9877–9882.
356. Shim BS, Tang Z, Morabito MP, Agarwal A, Hong H, Kotov NA. Integration of conductivity, transparency, and mechanical strength into highly homogeneous layer-by-layer composites of single-walled carbon nanotubes for optoelectronics. *Chem Mater.* 2007;19:5467–5474.
357. Elechiguerra JL, Larios-Lopez L, Liu C, Garcia-Gutierrez D, Camacho-Bragado A, Yacamán MJ. Corrosion at the nanoscale: the case of silver nanowires and nanoparticles. *Chem Mater.* 2005;17:6042–6052.
358. Zhao J, Sun H, Dai S, Wang Y, Zhu J. Electrical breakdown of nanowires. *Nano Lett.* 2011;11:4647–4651.
359. Thostenson ET, Li C, Chou T-W. Nanocomposites in context. *Compos Sci Technol.* 2005;65:491–516.
360. Jackson R, Domercq B, Jain R, Kippelen B, Graham S. Stability of doped transparent carbon nanotube electrodes. *Adv Funct Mater.* 2008;18:2548–2554.
361. Hellstrom SL, Vosgueritchian M, Stollenberg RM, et al. Strong and stable doping of carbon nanotubes and graphene by MoO₃ for transparent electrodes. *Nano Lett.* 2012;12:3574–3580.
362. Zhou Y, Shimada S, Saito T, Azumi R. Building interconnects in carbon nanotube networks with metal halides for transparent electrodes. *Carbon.* 2015;87:61–69.
363. Dobbertin T, Kroeger M, Heithecker D, et al. Inverted top-emitting organic light-emitting diodes using sputter-deposited anodes. *Appl Phys Lett.* 2003;82:284–286.
364. Kim H-K, Kim D-G, Lee K-S, et al. Plasma damage-free sputtering of indium tin oxide cathode layers for top-emitting organic light-emitting diodes. *Appl Phys Lett.* 2005;86:183503.
365. Parthasarathy G, Burrows P, Khalfin V, Kozlov V, Forrest S. A metal-free cathode for organic semiconductor devices. *Appl Phys Lett.* 1998;72:2138–2140.
366. Burrows P, Gu G, Forrest S, Vicenzi E, Zhou T. Semitransparent cathodes for organic light emitting devices. *J Appl Phys.* 2000;87:3080–3085.
367. Gu G, Parthasarathy G, Burrows P, et al. Transparent stacked organic light emitting devices. I. Design principles and transparent compound electrodes. *J Appl Phys.* 1999;86:4067–4075.
368. Kim D, Han Y, Cho J-S, Koh S-K. Low temperature deposition of ITO thin films by ion beam sputtering. *Thin Solid Films.* 2000;377:81–86.
369. Hoshi Y, Kiyomura T. ITO thin films deposited at low temperatures using a kinetic energy controlled sputter-deposition technique. *Thin Solid Films.* 2002;411:36–41.
370. Lagrange M, Langley D, Giusti G, Jiménez C, Bréchet Y, Bellet D. Optimization of silver nanowire-based transparent electrodes: effects of density, size and thermal annealing. *Nanoscale.* 2015;7:17410–17423.
371. Kwan YCG, Le QL, Huan CHA. Time to failure modeling of silver nanowire transparent conducting electrodes and effects of a reduced graphene oxide over layer. *Sol Energy Mater Sol Cells.* 2016;144:102–108.
372. Kholmamov IN, Domingues SH, Chou H, et al. Reduced graphene oxide/copper nanowire hybrid films as high-performance transparent electrodes. *ACS Nano.* 2013;7:1811–1816.
373. Song T-B, Rim YS, Liu F, et al. Highly robust silver nanowire network for transparent electrode. *ACS Appl Mater Interfaces.* 2015;7:24601–24607.
374. Kim T, Canlier A, Kim GH, Choi J, Park M, Han SM. Electrostatic spray deposition of highly transparent silver nanowire electrode on flexible substrate. *ACS Appl Mater Interfaces.* 2013;5:788–794.
375. Nan HY, Ni ZH, Wang J, Zafar Z, Shi ZX, Wang YY. The thermal stability of graphene in air investigated by Raman spectroscopy. *J Raman Spectrosc.* 2013;44:1018–1021.
376. Hu Z, Zhang J, Hao Z, Hao Q, Geng X, Zhao Y. Highly efficient organic photovoltaic devices using F-doped SnO₂ anodes. *Appl Phys Lett.* 2011;98:66.
377. Liu M, Johnston MB, Snaith HJ. Efficient planar heterojunction perovskite solar cells by vapour deposition. *Nature.* 2013;501:395.
378. Lee MM, Teuscher J, Miyasaka T, Murakami TN, Snaith HJ. Efficient hybrid solar cells based on meso-superstructured organometal halide perovskites. *Science.* 2012;338:643–647.
379. Burschka J, Pellet N, Moon S-J, et al. Sequential deposition as a route to high-performance perovskite-sensitized solar cells. *Nature.* 2013;499:316.
380. Formica N, Ghosh DS, Chen TL, Eickhoff C, Bruder I, Pruneri F. Highly stable Ag–Ni based transparent electrodes on PET substrates for flexible organic solar cells. *Sol Energy Mater Sol Cells.* 2012;107:63–68.
381. Wu E-E, Li S-H, Chen C-W, Li G, Xu Z, Yang Y. Controlling optical properties of electrodes with stacked metallic thin films for polymeric light-emitting diodes and displays. *J Disp Technol.* 2005;1:105–111.
382. Stee HM, Williams RJ, Jones TS, Hutton RA. Ultrathin transparent Au electrodes for organic photovoltaics fabricated using a mixed mono-molecular nucleation layer. *Adv Funct Mater.* 2011;21:1709–1716.
383. Schubert S, Meiss J, Müller-Meskamp L, Leo K. Improvement of transparent metal top electrodes for organic solar cells by introducing a high surface energy seed layer. *Adv Energy Mater.* 2013;3:438–443.
384. Kang MG, Guo LJ. Nanoimprinted semitransparent metal electrodes and their application in organic light-emitting diodes. *Adv Mater.* 2007;19:1391–1396.
385. Rowell MW, Topinka MA, McGehee MD, et al. Organic solar cells with carbon nanotube network electrodes. *Appl Phys Lett.* 2006;88:233506.
386. Feng Y, Ju X, Feng W, et al. Organic solar cells using few-walled carbon nanotubes electrode controlled by the balance between sheet resistance and the transparency. *Appl Phys Lett.* 2009;94:90.
387. Kim S, Yim J, Wang X, Bradley DD, Lee S, deMello JC. Spin-and spray-deposited single-walled carbon-nanotube electrodes for organic solar cells. *Adv Funct Mater.* 2010;20:2310–2316.
388. Yang Z, Chen T, He R, et al. Aligned carbon nanotube sheets for the electrodes of organic solar cells. *Adv Mater.* 2011;23:5436–5439.
389. Zhang D, Choy WC, Wang CC, et al. Polymer solar cells with gold nanoclusters decorated multi-layer graphene as transparent electrode. *Appl Phys Lett.* 2011;99:259.
390. Lin P, Choy WC, Zhang D, Xie F, Xin J, Leung C. Semitransparent organic solar cells with hybrid monolayer graphene/metal grid as top electrodes. *Appl Phys Lett.* 2013;102:49.



Xiaoyue Li received a Bachelor of Science degree from China Agricultural University (China) in 2014 and a Ph.D. in inorganic chemistry from Peking University (China) in 2019. She is currently working at the Department of Materials and Engineering of the University of Toronto (Canada) as a postdoctoral fellow, funded by Yunnan University Faculty-track International Postdoctoral Fellow. Her current research is on developing functional materials for organic light-emitting diodes (OLEDs) and photovoltaic cells.



Zheng-Hong Lu is a professor and a Tier I Canada Research Chair in Organic Optoelectronics at the Department of Materials Science and Engineering of the University of Toronto and is a visiting professor at Southern University of Science and Technology and Yunnan University. Prof. Lu has been working on and has made numerous seminal contributions on surfaces, interfaces, thin-films and optoelectronic devices. He was elected as a fellow of AAAS in 2016, a fellow of the Canadian Academy of Engineering in 2017, and a fellow of the Academy of Science division of the Royal Society of Canada in 2019.